Seasonal characteristics of trace gas transport into the extratropical upper troposphere/lower stratosphere

Yoichi Inai[1], Ryo Fujita[2,1], Toshinobu Machida[3], Hidekazu Matsueda[4], Yousuke Sawa[4], Kazuhiro Tsuboi[4], Keiichi Katsumata[3,5], Shinji Morimoto[1], Shuji Aoki[1], Takakiyo Nakazawa[1]

[1] Center for Atmospheric and Oceanic Studies, Graduate School of Science, Tohoku University, Sendai, 980-8578, Japan
[2] Department of Physics, Imperial College London, South Kensington Campus, London SW7 2AZ, United Kingdom
[3] National Institute for Environmental Studies, Tsukuba, 305-8506, Japan
[4] Meteorological Research Institute, Tsukuba, 305-0052, Japan
[5] Now at Takachiho Chemical Industrial Co., Ltd., Tokyo, 194-0004, Japan

Correspondence to: Yoichi Inai (yoichi_inai@tohoku.ac.jp)

Abstract. To investigate the seasonal characteristics of trace gas distributions in the extratropical upper troposphere and lower stratosphere (ExUTLS) as well as stratosphere–troposphere exchange processes, origin fractions of air masses originating in the stratosphere, tropical troposphere, mid-latitude lower troposphere (LT), and high-latitude LT in the ExUTLS are estimated using 10-year backward trajectories calculated with European Centre For Medium-Range Weather Forecasts (ECMWF) ERA-Interim data as the meteorological input. Time-series of trace gases obtained from ground-based and airborne observations are incorporated into the trajectories, thus reconstructing spatiotemporal distributions of trace gases in the ExUTLS. The reconstructed tracer distributions are analysed with the origin fractions and the stratospheric age of air (AoA) estimated using the backward trajectories. The reconstructed distributions of CO and CO_2 in the ExUTLS are affected primarily by tropospheric air masses because of the short chemical lifetime of the former and large seasonal variations in the troposphere of the latter. Distributions of CH_4, N_2O, and SF_6 are controlled primarily by seasonally varying air masses transported from the stratosphere. For CH_4 and N_2O distributions, chemical decay along the average path from the source region is particularly important.

1 Introduction

The extra-tropical upper troposphere and lower stratosphere (ExUTLS; e.g., Gettelman et al., 2011) accounts for about 40 % of the total stratospheric air mass (Appenzeller et al., 1996) and about 20 % of stratospheric aerosols (Andersson et al., 2015). Trace gases and aerosols in the ExUTLS play an important role in atmospheric radiative processes. These species are transported to the ExUTLS from the deep stratosphere via stratospheric circulation (Brewer–Dobson circulation, BDC; Brewer, 1949; Dobson, 1956) and from the lower troposphere or the tropical troposphere via local convection, frontal cyclones, Rossby wave breaking at/along the subtropical jet, monsoon activity, and other systems (e.g., Holton et al., 1995; Wernli and Bourqui, 2002; Manney et al., 2011; Pan et al., 2016; Vogel et al., 2016; Boothe and Homeyer, 2017; Ploeger et al., 2017).

Air-mass transport processes into the ExUTLS are strongly dependent on the season. This leads to stratospheric and tropospheric mixing fractions that show clear seasonality. For example, Appenzeller et al. (1996) estimated the mass flux across the 380 K isentrope due to global-scale meridional circulation and found that the downwelling mass flux from the stratosphere varies from 8×10^9 kg s^{-1} in summer to 15×10^9 kg s^{-1} in winter, whereas the Asian summer monsoon and local

5   convection, which supply tropospheric air to the ExUTLS, are active only during the summer and early autumn (e.g., Randel and Park, 2006; Randel et al., 2010). The composition of air masses transported from the deep stratosphere, lower troposphere, and tropical troposphere also shows seasonal variations (e.g., Boenisch et al., 2009). The seasonal variability in air-mass composition and mass-flux strength makes it difficult to essentially understand the distributions of trace gases in the ExUTLS and to describe their transport into the layer.

10 This study focuses on mixing fractions of air masses originating in the stratosphere, tropical troposphere, mid-latitude lower troposphere (LT), and high-latitude LT (hereafter, referred to as "origin fractions") in the ExUTLS, based on the trajectory analysis of Inai (2018). Using estimated origin fractions, the transport of chemical species into the ExUTLS and the spatiotemporal distributions of methane (CH_4), nitrous oxide (N_2O), carbon monoxide (CO), sulphur hexafluoride (SF_6), and carbon dioxide (CO_2) in the layer are reconstructed with the aid of atmospheric trace gas observations including aircraft

15 measurements, such as those of the Comprehensive Observation Network for TRace gases by AIrLiner (CONTRAIL; Nakazawa et al., 1993; Matsueda and Inoue, 1996; Ishijima et al., 2001; Matsueda et al., 2002; Machida et al., 2008; Umezawa et al., 2014; Sawa et al., 2015). Reconstructed distributions for the five species are discussed in terms of dynamical transport as well as chemical loss, using the stratospheric age of air (AoA) as an indicator of air mass transport via the deep and shallow branches of the BDC.

20 **2 Methods**

2.1 Estimating the origin fraction and age of air

The CONTRAIL data were obtained by collecting air samples once a month from April 2012 to December 2016 at longitudinal intervals of 10° or 15° along individual flight tracks at around 11 km altitude between France/Russia and Japan. The period and longitudinal locations of this analysis were selected based on the CONTRAIL measurements, for which air sampling in

25 the ExUTLS was usually made over Siberia. To identify the origins of ExUTLS air masses, kinematic backward trajectories are calculated for 10 years following the method of Inai (2018). Trajectories are initialized at uniformly distributed grid points (5.0° longitude × 2.5° latitude) within 45° N–80° N and 0° E–140° E at geopotential heights of 5, 6, 7, 8, 9, 10, 11, 12, 13, 14, 15, and 16 km (Fig. 1). Initializations are made at 00:00 UTC on the 5th, 15th, and 25th of every month from January 2012 to December 2016, and use meteorological conditions prescribed by the European Centre for Medium-Range Weather Forecasts

30 (ECMWF) ERA-Interim dataset (1.5° × 1.5° horizontal resolution, 6 hourly temporal resolution, and 37 pressure levels; Dee et al., 2011). Although trajectories could be released at the exact CONTRAIL measurement locations and times, the grating initialization is employed because this study attempt to obtain uniform spatiotemporal tracer distributions as well as their

transports by capitalizing on the CONTRIAL measurements. An example of the results is provided in Fig. 2, which shows where particles located as shown in Fig. 1 at 00Z on 15 January 2015 were located 361 days prior (i.e., 00Z on 19 January 2014). Many particles ending up at altitudes greater than 13 km (orange dots) travelled from the stratosphere, above 18 km. However, many particles ending up at altitudes below 10 km (purple to blue-green dots) distribute below 15 km, typically in

5   the troposphere. Although the accuracy of individual trajectories is limited by the long-term nature of the calculations, statistical features of air-mass transport can be investigated using a large number of trajectories.

Trajectories obtained from each run are categorized into several groups (trj_k; k = 1 to $kmax$) with criteria (hereafter denoted cri_k) of potential temperature, latitude, potential vorticity, and geopotential height along each trajectory. In this analysis, $kmax$ is set to 4, with k = 1 for the stratosphere, k = 2 for the tropical troposphere, k = 3 for the mid-latitude LT, and k = 4 for the

10   high-latitude LT. Criteria for each k are summarized in Table 1. The trajectories are also used to determine whether trajectories categorized as $trj_{k=1}$ passed through the deep or shallow branch of the BDC (k = 1d or 1s). These trajectories are classified as shallow-branch if they cross 400 K but do not reach 30 hPa within 4 years, and as deep-branch if they exceed 30 hPa within 4 years, following the method of Lin et al. (2015). Trajectories were categorized as trj_k, according to the first set of 3 continuous days along the trajectory that satisfied the cri_k. This resulted in all trajectories being categorized as k = 1, 2, 3, or 4 within 10

15   years. Trajectories trj_k are assumed to travel along unique paths from origin k to the initial position of the backward trajectory. Origin fractions of air parcels with origin k (hereafter denoted f_k) are calculated as a function of equivalent latitude ($\emptyset_{eq}$), potential temperature (θ), and month ($\mathcal{M}$) of their release. Denoting as N_k the number of trajectories, which are classified into trj_k groups with distinct $\emptyset_{eq}$, θ, and $\mathcal{M}$, the origin fraction for origin k is given by

$$f_k = \frac{\sum_{i=1}^{N_k} \rho_{trj_k ini}(i) * \cos \emptyset_{trj_k ini}(i)}{\sum_{k=1}^{kmax}(\sum_{i=1}^{N_k} \rho_{trj_k ini}(i) * \cos \emptyset_{trj_k ini}(i))}, \tag{1}$$

20   where $\emptyset_{trj_k ini}$ and $\rho_{trj_k ini}$ indicate the initial latitude and density of the individual backward trajectories, respectively. Note that $\rho_{trj_k ini}$ is calculated from the equation of state. Results of a sensitivity analysis indicate that the estimated origin fractions are independent of the resolution of the input meteorological data (see Appendix A).

Similar methods are used to estimate the AoA, which is calculated as the average elapsed time until a trajectory goes back to the troposphere where it satisfies whichever criteria k = 2, 3, or 4. Thus, the AoA definition used here differs from that of Hall

25   and Plumb (1994), who defined AoA as the elapsed time an air parcel spends in the stratosphere after across the tropopause. In our estimates of AoA, however, a small fraction of trajectories are still in the stratosphere at the end of the 10-year calculation. Figure 3 shows the percentage of such remaining trajectories estimated as a function of $\emptyset_{eq}$, θ, and $\mathcal{M}$ of their release. The percentages are almost zero in the region where potential vorticity is <4 PVU, whereas they are generally non-zero in the region where potential vorticity is >4 PVU. However, even in this region the values are <2.5 %. Here, we define ε as the

30   percentage of trajectories that are still in the stratosphere after the 10-year backward calculation as a function of $\emptyset_{eq}$, θ, and $\mathcal{M}$ (Fig. 3). Then, the AoA (Γ_{Trj}) is obtained using the elapsed time since each trajectory $trj_k(i)$ left its origin k ($\equiv \tau_k(i)$) according to

$$\Gamma_{Trj} = \sum_{k=2}^{4} \frac{\sum_{i=1}^{N_k} \gamma TT * \tau_k(i) * \rho_{trj_k ini}(i) * \cos \emptyset_{trj_k ini}(i)}{\sum_{i=1}^{N_k} \rho_{trj_k ini}(i) * \cos \emptyset_{trj_k ini}(i)} * (1 - \varepsilon) + \overline{\Gamma_{tail}} * \varepsilon, \tag{2}$$

where $\overline{\Gamma_{tail}}$ is the average AoA for air parcels remaining in the stratosphere longer than the maximum length of the trajectory calculation tf (= 10 years), calculated as follows:

$$\overline{\Gamma_{tail}} = \frac{\int_{\gamma TT * tf}^{\infty} \tau' * PDF(\tau') * \exp\left(-b*(\tau' - \gamma TT * tf)\right) d\tau'}{\int_{\gamma TT * tf}^{\infty} PDF(\tau') * \exp\left(-b*(\tau' - \gamma TT * tf)\right) d\tau'}, \tag{3}$$

$$= (\gamma TT * tf + \frac{1}{b}), \tag{3'}$$

where PDF is the age probability distribution function or "age spectrum," and b is the exponential decay parameter of the PDF, with its value (b = 0.2038 yr^{-1}) from Diallo et al. (2012). The decay parameter in the present analysis may differ from that used by Diallo et al. (2012) because of differences in the vertical trajectory calculations (i.e., kinematic in the present study and diabatic in their work). However, this difference is expected to have little impact on the results because ε is small, as shown in Figure 3. The term γTT in Eqs (3 and 3') is a correction factor for τ_k and is required because previous studies (e.g., Inai, 2018) have found that the AoA estimated by trajectory analysis using ERA-Interim data is underestimated, particularly when using a kinematic treatment. Inai (2018) found that this underestimation corresponds to 70 % of the observed value in the mid-latitude stratosphere. To address this underestimation, the AoA values calculated here are corrected by comparing with AoA derived from SF$_6$ mixing ratios (Γ_{SF6}) assuming a linear trend relative to the time series at Mauna Loa (https://www.esrl.noaa.gov/gmd/obop/mlo/) of 0.33 ppt yr^{-1} (ppt: parts per trillion by mole, with similar definitions for ppm and ppb). When γTT is set at 1.5, Γ_{Trj} agrees well with Γ_{SF6} (Fig. 4). Thus, a value of 1.5 was used for γTT in this study. The AoA for air masses originating in the stratosphere and those that passed through the deep and shallow branches of the BDC were evaluated using $trj_{k=1}$, $trj_{k=1d}$, and $trj_{k=1s}$, respectively. Note that because this study performs a trajectory analysis using an objective reanalysis dataset, subgrid-scale processes, such as the sporadic injection of tropospheric air masses into the ExUTLS, cannot be explicitly reproduced. Thus, to remove the influence of such events, CONTRAIL data with CO mixing ratios higher than 80 ppb in the region above 340 K and north of 60° N equivalent latitude are not used in this comparison (the same criteria are applied to the comparison shown in Fig. 8 in Sect. 2.2.2).

2.2 Air-mass original composition and reconstruction

2.2.1 Reconstruction without chemical loss (step 1)

The relative abundance of chemical species in the ExUTLS is strongly affected by changes in the breakdown of transported air masses, reflecting the fact that air-mass chemical composition varies with origin. For example, low-latitude tropospheric air masses have relatively high N$_2$O mixing ratios, whereas high-latitude stratospheric air masses have low mixing ratios, because N$_2$O sources and sinks exist in the troposphere and the stratosphere, respectively. This study attempts to reconstruct the spatiotemporal distributions of the chemical species CH$_4$, N$_2$O, CO, SF$_6$, and CO$_2$, in the following two steps.

First, the chemically passive tracers (i.e., SF_6 and CO_2) are reconstructed. According to Inai (2018), if there is no chemical loss for S, the mixing ratio of chemical species S in the ExUTLS (X^S_{NoChem}) can be reconstructed as a function of $\emptyset_{eq}$, θ, and $\mathcal{M}$ in combination with f_k and the chemical transport from origin k (X^S_k):

$$X^S_{NoChem} = \sum_{k=1}^{kmax} f_k * X^S_k. \tag{4}$$

As the time series X^S_k should be treated climatologically for each k and S, as required for the origin fraction f_k, it is necessary to detrend their values. Therefore, the seasonality and trend of the mixing ratio of S are separately treated in this study. By expressing the detrended mixing ratio of S for an air mass originating in region k ($\equiv X^S_{ORG_k}$) as a function of month ($\equiv \mathcal{M}_{ORG}(i)$) when trajectory $trj_k(i)$ goes back to origin k after its advection during $\gamma TT * \tau_k(i)$ and assuming the tropospheric linear trend ($\equiv \lambda^S$), X^S_{NoChem} is calculated as a function of $\emptyset_{eq}$, θ, and $\mathcal{M}$ as follows:

$$X^S_{NoChem} = \sum_{k=2}^{4} \frac{\sum_{i=1}^{N_k} \left(X^S_{ORG_k}(\mathcal{M}_{ORG}(i)) - \lambda^S * \gamma TT * \tau_k(i) \right) * \rho_{trj_k ini(i)} * \cos\emptyset_{trj_k ini(i)}}{\sum_{i=1}^{N_k} \rho_{trj_k ini(i)} * \cos\emptyset_{trj_k ini(i)}} * (1 - \varepsilon) + \overline{X^S_{tail}} * \varepsilon, \tag{5}$$

where $\overline{X^S_{tail}}$ is average mixing ratio of S for air parcels remaining in the stratosphere more than tf and is calculated as follows:

$$\overline{X^S_{tail}} = \frac{\int_{\gamma TT * tf}^{\infty} (\chi_{2016} - \lambda^S * \tau\prime) * PDF(\tau') * \exp\left(-b * (\tau' - \gamma TT * tf)\right) d\tau\prime}{\int_{\gamma TT * tf}^{\infty} PDF(\tau\prime) * \exp\left(-b * (\tau' - \gamma TT * tf)\right) d\tau\prime}, \tag{6}$$

$$= \chi^S_{2016} - \lambda^S * \left(\gamma TT * tf + \frac{1}{b}\right). \tag{6'}$$

For $X^S_{ORG_k}$, detrending is applied to the observed values for $k = 2$, 3, and 4 in which a linear trend is determined for each dataset for the period 2012–2016 and all the observed values are normalized to those on January 2016. Monthly aircraft measurement data collected by Tohoku University (TU; Nakazawa et al., 1993; Ishijima et al., 2001; Umezawa et al., 2014) at around 2 km over the Pacific Ocean off the coast of Sendai, Japan are employed for $k = 3$ after taking a 3-month running average. For $k = 2$, an average of the data observed at ~11 km over 0° N–20° N using aircraft flying between Japan and Australia (Matsueda and Inoue, 1996; Matsueda et al., 2002) and the measurement data used for $k = 3$ are used. This averaging is required to account for underestimations of vertical transport from the LT in the trajectory analysis. This underestimation is discussed in more detail in Sect. 4.3. For $k = 4$, ground-based monthly mean data measured by NOAA/ESRL (National Oceanic and Atmospheric Administration/Earth System Research Laboratory) at Summit, Greenland (SUM) and Barrow, Alaska (BRW) are used after averaging the data from the two stations. N_2O and SF_6 data at both sites, and CH_4 and CO_2 data at BRW were continuously measured in situ, whereas other data were obtained using a flask sampling method (Dutton et al., 2017; Thoning et al., 2017; Dlugokencky et al., 2018a, 2018b, 2018c; Petron et al., 2018). These data are distributed by the World Meteorological Organization (WMO) World Data Centre for Greenhouse Gases (WDCGG; https://gaw.kishou.go.jp/). The χ^S_{2016} in Eqs (6 and 6') is assigned the mixing ratio of S for the mid-latitude LT ($k = 3$) after annual averaging for 2016. For the trend λ^S, 9.3 ppb yr^{-1} for CH_4, 1.0 ppb yr^{-1} for N_2O, 0.33 ppt yr^{-1} for SF_6, 2.3 ppm yr^{-1} for CO_2, and no trend for CO are assumed by reference to each time series from Mauna Loa (https://www.esrl.noaa.gov/gmd/obop/mlo/).

Figure 5 compares the reconstructions for CH_4, N_2O, CO, SF_6, and CO_2 and the CONTRAIL measurements after spatial interpolation to each measurement point for each month. The reconstructions for SF_6, and CO_2 generally agree with the

measurements, with some outliers during the summer season. In particular, some observed CO_2 mixing ratios have much smaller values than the reconstructions during boreal summer (Fig. 5e). This might be caused by CO_2 absorption by the local Eurasian forest and enhanced subgrid-scale vertical transport (e.g., local convection) during summer. The reconstructions for other seasons, however, generally agree with the CONTRAIL measurements. In contrast to SF_6 and CO_2, reconstructions for chemically active species (i.e., CH_4, N_2O, and CO) overestimate the CONTRAIL measurements. Because this overestimation is likely due to chemical loss along their path from the origin region to the ExUTLS, in the next step we perform a reconstruction while taking chemical loss into account.

2.2.2 Reconstruction with chemical loss (step 2)

The mixing ratios of chemically active species (CH_4, N_2O, and CO) are reconstructed using a simple model wherein each chemical loss is simulated along the path from its source region to the ExUTLS. Although each trajectory trj_k has a unique path and transit time from its origin k, an "average path" (AP; Schoeberl et al., 2000) can be defined by a cluster of such trajectories. In this study, APs are incorporated into the analysing framework using trajectories binned as a function of $\emptyset_{eq}$, θ, and $\mathcal{M}$. Because both the AP and AoA are defined using the same cluster of trajectories, the two values are considered to be consistent with each other. The relationship between AoA and the chemical loss rate is determined from observation results of Volk et al. (1997), who presented correlations between CH_4 and N_2O mixing ratios and AoA as well as the gradient of the mixing ratios with respect to AoA (figure 6a of their paper). Using their results, a relationship between the chemical decay and AoA is assumed, as shown in Fig. 6. The gradient of N_2O mixing ratio with respect to the AoA grows by -3 % yr^{-1} a year, whereas that for CH_4 is constant at -7 % yr^{-1} when the AoA is <2.5 years and becomes -11 % yr^{-1} when the AoA is >3.4 years. Using the assumed chemical decay, the relative abundances of CH_4 and N_2O are calculated (Fig. 6) and are found to agree well with the observed mixing ratios shown in figure 6a of Volk et al. (1997). The correlation between CO mixing ratio and AoA is not shown in their paper, so here it is assumed that the gradient of CO mixing ratio with respect to AoA is 20-times larger than that of CH_4. The expected relative abundance of CO with respect to AoA is also evaluated (Fig. 6).

To adapt the correlations between chemical decay and AoA (Fig. 6) to an AP, the chemical decay with respect to AoA is converted to an average loss rate with respect to transit time along an AP (TT$_{AP}$). Figure 7 shows the converted loss rates along an AP for the three tracers as well as the corresponding e-folding time. The converted loss rates produce the same relationships between the chemical decay and AoA shown in Fig. 6 if each species is reduced during TT$_{AP}$ with the given e-folding time as a function of TT$_{AP}$. Using these e-folding times ($\equiv \tau_{AP}^S$), the mixing ratio of chemically active species S after travelling an AP ($\equiv X^S$) is calculated as follows:

$$X^S = X_{NoChem}^S * \exp(-\frac{\Gamma_{Trj}}{\gamma_{Loss}^S * \tau_{AP}^S}),$$ (7)

where γ_{Loss}^S is a correction factor for τ_{AP}^S and is determined as follows. Because chemical loss rates might change with the season, we determine a correction factor for each month, such that the reconstruction X^S agrees with CONTRAIL measurements. Scatter plots of CONTRAIL measurements versus reconstructions (Fig. 8) are linear with a slope of 1.0 for

each month when the correction factors for CH_4 and N_2O are those shown in Fig. 9. Because the scatter plots have large dispersion for CO, instead of the slope, the difference between the CONTRAIL measurements and reconstructions is used for the determination of γ_{Loss}^S to minimize the difference. Thus, CH_4, N_2O, CO, SF_6, and CO_2 in the ExUTLS are reconstructed for a whole year ($X^S = X_{NoChem}^S$ for SF_6 and CO_2) and are summarised in Appendix B together with the origin fractions and

5   AoA. The detailed descriptions about them are made in the next section. As in the estimation of Γ_{Trj} for stratospheric air masses, the original mixing ratio S of air masses originating in the stratosphere $X^S{}_{ORG_{k=1}}$ is evaluated using only $trj_{k=1}$. The seasonal dependence of γ_{Loss}^S (i.e., the relative rate of chemical loss) estimated here is discussed in Sect. 4.2.

3 Results

3.1 Origin fraction

10   Distributions of origin fractions in a $\varnothing_{eq}-\theta$ cross-section are shown in Fig. 10 for January together with the climatology of monthly average potential vorticity for the period 2012–2016 obtained from ERA-Interim. In winter, origin fractions of the stratosphere dominate regions north of 40° N and higher than 340 K in altitude. In particular, regions where the altitude and equivalent latitude are greater than 360 K and 50° N, respectively, are almost entirely occupied by stratospheric air masses, further, that via the deep branch of the BDC shares roughly 30 % of the regions where the potential vorticity exceeds ~10 PVU

15   (Fig. 10c). However, origin fractions of the tropical troposphere dominate regions of lower latitude and altitudes where the potential vorticity is less than ~4 PVU. These origin fractions are >50 %, except in regions lower than 320 K in altitude. Air masses in regions lower than 310 K generally originate in the mid-latitude LT with mixing fractions up to ~70 %, with few air masses originating in the high-latitude LT.

The origin fractions for April are shown in Fig. 11. In spring, origin fractions of the stratosphere are similar to their winter

20   values, and dominate regions north of 40° N and higher than 340 K in altitude. Origin fractions of the stratosphere via the shallow branch of the BDC become slightly smaller than during winter, and those of the deep stratosphere via the deep branch of the BDC increase instead. Tropical tropospheric air masses continue to dominate regions where the potential vorticity is less than ~4 PVU at equivalent latitudes below 50° N, except for regions below 320 K where mid-latitude air masses are present. Origin fractions of the high-latitude LT remain small during spring.

25   Estimated origin fractions for July are shown in Fig. 12. In summer, origin fractions of the stratosphere become less dominant. In particular, those originating in the deep branch of the BDC (Fig. 12c) are small over the whole ExUTLS. Stratospheric air masses, almost all of which originate in the shallow branch of the BDC, are generally distributed in a small region where the altitude and equivalent latitude are greater than ~370 K and 40° N exceeding 50% of the origin fraction. In contrast, there is expansion of the region in which the origin fractions of the tropical troposphere are dominant. In particular, nearly 80 % of the

30   air masses in the region above 340 K and south of 40° N originate in the tropical troposphere. Only during this season do origin fractions of air masses originating in the high-latitude LT reach up to ~70 %, but these are limited to a region below ~320 K.

Origin fractions of the mid-latitude LT become smaller than during spring, but the region where they are higher than 30 % expands up to 340 K at all equivalent latitudes.

Origin fractions for October are shown in Fig. 13. During autumn, high origin fractions of the stratosphere broaden again in the region above 360 K. However, those originating in the deep branch of the BDC are small. Origin fractions of the high-latitude LT are suppressed, and the region where origin fractions of the tropical troposphere are higher than 50 % becomes larger than during summer and extends up to 80° N along 330–340 K potential temperature surfaces. In the region below 325 K, mid-latitude LT air masses dominate. These seasonal results are compared with previous studies in Sect. 4.1. The robustness and limitations of our estimates are discussed in Sect. 4.3.

3.2 Original composition and AoA

As described in Sect. 2.2, detrended mixing ratios of CH_4, N_2O, CO, SF_6, and CO_2 observed in the tropical troposphere, mid-latitude LT, and high-latitude LT are assigned to their original mixing ratios for $k = 2$, 3, and 4, respectively. For $k = 1$, the original mixing ratios are estimated by Eqs (5 and 6) using trajectories $trj_{k=1}$ for passive tracers and APs, and Eq. (7) for chemically active species. Figure 14 shows the original mixing ratios of each species assigned to an individual trajectory according to Eq. (5). Whereas CH_4 and SF_6 show seasonal variations and latitudinal gradients in the troposphere, N_2O does not. In contrast to the troposphere, CH_4 and N_2O in stratospheric air masses show distinct seasonal variations but somewhat different phase, with a minimum in boreal summer and maximum in winter for CH_4, and a minimum in boreal spring/summer and maximum in autumn/winter for N_2O. SF_6 mixing ratios are significantly smaller in stratospheric air masses than in the troposphere throughout the year, and show seasonal variations with a maximum in September and minimum in March. Note that these values for stratospheric air masses are estimated based on their final state, unlike the case for regions k = 2, 3, and 4, for which the values correspond to their original state. For CO, there are large seasonal variations in high- and mid-latitude tropospheric air masses, but tropical tropospheric values show smaller seasonal variations. The CO mixing ratios for the stratosphere show a slight seasonal variability, but are less than ~30 ppb throughout the year. For CO_2, seasonal variations are largest in the high-latitude troposphere; mixing ratios in the stratosphere show small seasonal variations, but with a phase that differs from that in the troposphere.

The estimated AoA of stratospheric air masses is shown in Fig. 14f. Stratospheric air masses transported via the deep branch of the BDC have AoA exceeding 5 years, whereas those transported via the shallow branch have AoA of 1–1.5 years. The average AoA among air masses originating in both branches shows a seasonal variation, with maximum values of ~2.7 years in March and minimum values of ~1.9 years in September, of almost opposite phase to that of SF_6 mixing ratios. The relationship between the original composition of stratospheric air masses and their AoA is discussed in Sect. 4.2.

3.3 Reconstructions

Chemical distributions reconstructed in the manner described in Sect. 2.2 are shown for January (Fig. 15) together with observation results obtained from CONTRAIL measurements over Siberia and monthly average potential vorticity obtained

from the ERA-Interim dataset during the period from 2012 to 2016. Spatial distributions of all chemical species generally show higher mixing ratios with decreasing potential temperature, equivalent latitude, or potential vorticity. Conversely, the distribution of AoA generally shows a higher age with increasing potential temperature, equivalent latitude, or potential vorticity. In particular, an AoA of greater than 3 years is estimated in the deep ExUTLS for regions higher than 380 K and

5   north of 70° N.

The reconstructions and AoA for April (Fig. 16) show spatial distributions of all species that generally increase with decreasing potential temperature, equivalent latitude, or potential vorticity, as is the case for January. However, the gradients are larger, particularly for CH_4 and N_2O mixing ratios, such that in regions where the potential vorticity is >6 PVU the mixing ratios are much smaller than those in January, but in regions where the potential vorticity is <4 PVU the mixing ratios are almost the

10   same as in January. The AoA distribution has a structure similar to that shown for January; i.e., age that increases with potential temperature, equivalent latitude, or potential vorticity.

The spatial distributions of the chemical species and AoA change more during summer than during winter and spring (Fig. 17). In particular, all five chemical species show minima at ~350 K north of 60° N equivalent latitude. These minima might be formed by remainder of the deep stratospheric air masses which were transported during spring. The tracer minima near

15   ~350 K at high equivalent latitudes begin forming in June. This "sandwich" structure in the ExUTLS has been reported by Ploeger and Biner (2016) for summer and by Krause et al. (2018) for spring. In agreement with their studies, the sandwich structures can show evidence for strong poleward transport above ~400 K, leading to mixing ratio minima at lower altitudes. For CO_2, some CONTRAIL measurements show significantly lower mixing ratios than the reconstructed values. The difference between the CONTRAIL measurements and the reconstructions are discussed in Sect. 4.3. The AoA becomes

20   significantly smaller during this season compared with winter and spring. In particular, the AoA of nearly the entire region is <1.6 year with the exception of the region where the tracer minima are formed.

In autumn, the chemical gradients for CH_4, N_2O, SF_6, and CO_2 in the ExUTLS are reduced (Fig. 18), in large part because CH_4 and N_2O mixing ratios in the deeper ExUTLS increase up to 1750 ppb for CH_4 and 315 ppb for N_2O. The reconstructed CO_2 mixing ratios show a nearly homogeneous distribution in the ExUTLS, leading to a distribution of higher CO_2 air masses along

25   the 6–8 PVU potential vorticity surface. The spatial distribution of CO, however, retains a steep gradient, because its chemical lifetime is small (several months). The distribution of AoA during autumn is similar to that during summer, with the AoA of nearly the entire region with potential vorticity of <8 PVU being less than 1 year.

4 Discussion

30   One goal of the current study is to visualize how seasonal variations in air masses as well as trace gas transport affect the spatiotemporal distributions of chemical species in the ExUTLS. This is accomplished by determining the seasonal characteristics of origin fractions of ExUTLS air masses originating in each region k at fixed points with those of the

reconstructions for each species, and comparing the distribution of each species in the ExUTLS with the original mixing fraction in each origin region. We next discuss the results of this analysis and some implications revealed through the reconstructing procedures, together with the limitations of the current study.

4.1 Seasonal variations in origin fractions and reconstructions at fixed locations

5   To identify the characteristics of seasonal variations in origin fractions and reconstructions at fixed locations, four regions are selected: mid-equivalent latitude upper (MU) ExUTLS (45° N, 370 K), high-equivalent latitude upper (HU) ExUTLS (75° N, 370 K), mid-equivalent latitude lower (ML) ExUTLS (45° N, 320 K), and high-equivalent latitude lower (HL) ExUTLS (75° N, 320 K). Figure 19 shows seasonal variations in the origin fractions of each origin evaluated at the four locations. In the MU ExUTLS, origin fractions of the tropical troposphere become high, exceeding 50 % during summer and autumn.

10 Accompanying this increase, trajectories originating in the tropical troposphere over around Asia are strengthened. In the other seasons, origin fractions of the stratosphere dominate. In particular, those that travelled via the shallow branch of the BDC exceed 50 %. The origin fractions of the mid- and high-latitude LT are nearly zero throughout the year, with the exception of that for the mid-latitude LT in autumn. In the HU ExUTLS, origin fractions of the stratosphere dominate and exceed 60 % throughout the year. Furthermore, origin fractions of air masses that travelled via the deep branch of the BDC exceed 20 %

15 during the period from January to April, whereas tropical tropospheric air masses generally fail to reach this region during this period. In the ML ExUTLS, tropospheric origin fractions are dominant. In particular, those of the mid-latitude troposphere exceed 50 % during summer and those of the high-latitude troposphere exceed 20 % during July and August. During winter and spring, however, tropical tropospheric air masses dominate. In the HL ExUTLS, origin fractions of the mid- and high-latitude LT are enhanced during summer. Origin fractions of the high-latitude LT are comparable to those in the ML ExUTLS,

20 but smaller than those of the mid-latitude LT in the HL ExUTLS. This can be explained by enhanced exchange at the bottom edge of the subtropical jet (i.e., along the 320–330 K surface for summer, e.g., Gettelman et al., 2011). As shown in Fig. 12d, enhanced origin fractions of the mid-latitude LT are distributed along such isentropes. In winter, origin fractions of the tropical troposphere and stratosphere are roughly 50 % and 40 %, respectively.

In addition to seasonal variations in origin fractions, seasonal variations in the tracer mixing ratios in origin regions (Fig. 14)

25 also affect chemical distributions in the ExUTLS. Figure 20 reveals that seasonal variations in the reconstructions for each species and the trajectory-estimated AoA in each of the four locations have patterns that differ because they are based on a superposition of the origin fractions shown in Fig. 19 with the original time series for $k = 1$–4 of the individual tracers shown in Fig. 14. Note that the CONTRAIL data are plotted if the measurement was conducted within ±5° in equivalent latitude and within ±5 K in potential temperature of one of the four locations. This results in few plotted CONTRAIL observations in mid-

30 and HL ExUTLS regions during summer, and no observations in MU and HU ExUTLS regions from June to January. This is caused by the seasonality of the thermal and dynamical structures of the ExUTLS and fixed flight altitudes. Despite the sparse and non-uniform observational field, the spatiotemporal distributions of chemical species, together with the origin fractions of the original air masses, can be resolved. This ability is one of the important advantages of the current analysis. The mixing

ratios of CH_4 and N_2O show modest seasonal variations in the lower ExUTLS, whereas they show large seasonal variations in the upper ExUTLS, with minima in spring and maxima in autumn. The minima in spring are due to the transport of stratospheric air masses via the deep branch of the BDC, which have low CH_4 and N_2O mixing ratios and also low AoA. This seasonal variation in chemical abundance for stratospheric air masses is discussed further in the next section. In contrast to CH_4 and

5 N_2O, CO mixing ratios show smaller seasonal variations in the upper ExUTLS than in the lower ExUTLS, with the exception of the high mixing ratio in the upper ExUTLS in August. This can be explained by the transport of mid-latitude LT air masses, which have higher CO mixing ratios than the other air masses, to the lower ExUTLS during summer. In addition, a large fraction of air masses reach the upper ExUTLS only during August. The seasonal characteristics of SF_6 mixing ratios are similar to those of CH_4 and N_2O. The phase of seasonal variations in the upper ExUTLS is nearly synchronized with, but

10 slightly precedes, those of CH_4 and N_2O, and more closely resembles the upside-down pattern of AoA variations (Fig. 20f). The phase of seasonal variations of CO_2 mixing ratios in the lower ExUTLS is nearly synchronized between the ML and HL ExUTLS, with the largest amplitude being evident in the ML ExUTLS. The phase of CO_2 variations in the upper ExUTLS is quite different from that in the lower ExUTLS, with maxima during summer/autumn. This seasonal variation in the upper ExUTLS is consistent with observational estimates by Hoor et al. (2004) and Strahan et al. (2007).

15 Seasonal variations in AoA evaluated at the four locations are shown in Fig. 20f. The phase of seasonal variations for the four locations is roughly synchronized, whereas the absolute values are clearly different. For example, AoA in the HU ExUTLS has a maximum of >2.5 years during spring and a minimum of ~1.3 years during the end of summer, whereas in the ML ExUTLS the maximum is only ~0.5 years and occurs during the period from winter to spring. The amplitude of AoA variations in the ExUTLS is likely related to air-mass mixing from the stratosphere, particularly when this involves air masses that have

20 been transported via the deep branch of the BDC. This point is discussed further in the next section, in relation to seasonal variations in chemical composition.

4.2 Original compositions and mixing effects

As discussed in the previous section, the distributions of CO and CO_2 in the ExUTLS are strongly affected by tropospheric air masses because CO has a short chemical lifetime and CO_2 shows large seasonal variations in the high- and mid-latitude LT.

25 For CH_4, N_2O, and SF_6, however, seasonal variations in origin fractions of the stratospheric air masses and in the compositions of the original air masses are considered to be essential factors in their spatiotemporal distributions in the ExUTLS. Here, we discuss seasonal variations in the composition of stratospheric air masses and how this affects chemical distributions via mixing with tropospheric air masses in the ExUTLS. Figure 21 shows the relationships between chemical abundances from CONTRAIL measurements and the AoA estimated from the trajectories and interpolated to each CONTRAIL measurement

30 location, along with these relationships for each original air mass. The AoA for stratospheric air masses are the same as those shown in Fig. 14f, whereas the AoA for the tropical, mid- and high-latitude troposphere are set to zero. Thus, the denotations for the tropospheric air masses only move vertically in the cross-sections according to their seasonal variations. Overall, the CONTRAIL measurements are roughly distributed on lines connecting the tropospheric and stratospheric air masses for all

seasons and chemical compositions. This linear distribution suggests that dynamical mixing of tropospheric with stratospheric air masses shapes the chemical distributions of the ExUTLS. Such linear "mixing lines" also suggest that the mixing took place rapidly (i.e., at a time-scale shorter than their chemical lifetimes) along an isentropic surface (Plumb, 2007 and references therein). A comparison of the distribution of CONTRAIL measurements with trends in the troposphere for SF_6 shows that the

5   CONTRAIL measurements are distributed along the lines of the sign-reversed trend. According to Engel et al. (2002) and Bönisch et al. (2009), the mixing ratios of CO_2 and AoA do not correlate below a level of ~3 years AoA because the propagated signal of the tropospheric seasonal cycle into the stratosphere is still detectable. In agreement with their results, the CONTRAIL CO_2 measurements also converge to the sign-reversed trend with increasing AoA. However, for CH_4 and N_2O, measurements depart from the sign-reversed trends toward lower mixing ratios with increasing AoA. This deflection can be interpreted as

10   being due to their stratospheric sinks; i.e., chemical destruction of CH_4 and N_2O in the stratosphere, with no such destruction of SF_6 and CO_2.

Both the AoA and chemical abundance of the original air masses from the stratosphere show seasonal variations that might be caused by seasonal variations in mass fluxes from the deep and shallow branches of the BDC. Figure 21f shows seasonal variations in AoA and the value that is calculated by integration of "age spectrum" (PDF) from 0 to *tf* for air masses originating

15   in the stratosphere as well as those separately evaluated for air masses that have travelled via the deep and shallow branches of the BDC. As the PDF is calculated with a weighting factor according to area and density, as in Eq. (1), their integrations reveal relative masses. Air masses originating in both the shallow and deep branches have minima in September and maxima in March. These in-phase seasonal variations enhance both the seasonal variations of the total origin fractions of the stratosphere and its average AoA.

20   Interesting cyclic structures appear in CH_4 and N_2O mixing ratios and their AoAs in stratospheric air masses. For example, the CH_4 mixing ratio is ~1750 ppb (AoA of ~2.3 years) in winter, ~1700 ppb (AoA of ~2.6 years) in spring, ~1650 ppb (AoA of ~2.3 years) in summer, and again ~1700 ppb (AoA of ~2.0 years) in autumn. Thus, clockwise rotations are the result of this pattern. The same is true for stratospheric N_2O and AoA. These rotations are formed by seasonal variations in AoA that are at a maximum in spring and a minimum in autumn, in combination with seasonal variations in the relative chemical loss rate

25   along the AP (defined as γ_{Loss}^{S} and discussed in Sect. 2.2.2) that is at a maximum in winter and a minimum in summer. These $\pi/2$ phase-lagged seasonal variations result in rolling variations in the relationship between CH_4 and N_2O mixing ratios and AoA in stratospheric air masses. The seasonal variation in AoA is determined by the mixing of stratospheric air masses via the deep branch of the BDC (Fig. 21f). Although the mechanism driving the seasonality of the chemical loss rate along AP is unknown, it is likely involved that the seasonal change of the relationship between AP and AoA as a possible mechanism from

30   dynamical viewpoint. Other candidate mechanisms from a chemical viewpoint are seasonal changes in the abundance of disrupting substance along the AP, or seasonal changes in the solar radiation intensity and sunlit time.

The abundance of N_2O and CH_4 in stratospheric air mass may be related to the fraction of air masses travelling via the deep and shallow branches. The relationship between the chemical abundance and mass fraction of the two branches is now considered. The current study estimates approximately 24 % and 14 % of air masses following the deep branch are of

stratospheric origin in spring and autumn, respectively, and the AoA is estimated to be ~6.4 years (Fig. 21f). Andrews et al. (2001) estimated the N_2O mixing ratio in the mid-latitude deep stratosphere to be ~80 ppb and <40 ppb where the AoA is estimated from CO_2 mixing ratio to be 5.5 years and 6.0 years, respectively. As their estimates are normalized to 1997 tropospheric values, the quantitative difference in the baseline N_2O mixing ratios may differ by ~20 ppb from the present

5   values. If we assume the N_2O mixing ratio of air masses originating in the deep branch of the BDC is 60 ppb, and that air masses are mixed at ratios of 24 % and 14 % with air masses whose N_2O mixing ratio is 330 ppb, such mixing leads to ~265 ppb and ~290 ppb N_2O mixing ratios, respectively. These values are up to ~20 ppb lower than the N_2O mixing ratios of ~280 ppb in May and ~310 ppb in November estimated for the original stratospheric air masses shown in Figs 14b and 21b. The same arguments are valid for CH_4 with respect to the relationship between stratospheric CH_4 mixing ratios and AoA; i.e., CH_4

10   mixing ratios are <600 ppb in regions where the AoA is >5.5 years, as estimated by Röckmann et al. (2011). These overestimations of N_2O and CH_4 mixing ratios for the original stratospheric air masses might be due to overestimation of the AoA and/or overestimation of the origin fraction of air masses originating in the deep branch of the BDC. These possibilities are discussed further in the next section.

4.3 Limitations of the current study

15   This study provides a detailed explanation of seasonal variations in chemical distributions and transport in the ExUTLS from a dynamical standpoint using trajectory analysis in combination with aircraft measurements. Results suggest that the spatiotemporal distributions of CH_4, N_2O, SF_6, and AoA in the ExUTLS are controlled primarily by air-mass transport via the deep and shallow branches of the BDC and by their mixing with tropospheric air masses in the ExUTLS, whereas those of CO and CO_2 are controlled largely by tropospheric air masses, because CO has a short chemical lifetime and CO_2 shows large

20   seasonal variations in the mid-latitude LT. However, some assumptions and limitations of the current study should be mentioned.

First, some uncertainty results from the use of ERA-Interim data in trajectory analyses. Trajectory results generally depend on the resolution of the input data. We performed sensitivity analyses to clarify this dependency in our origin fraction estimates (Appendix A). Results confirm that our estimates are independent of the resolution of the ERA-Interim data, at least as they

25   relate to statistical characteristics. Furthermore, it is known that AoA calculated from trajectory analyses using ERA-Interim data are somewhat young-biased. For example, these estimated AoA values are ~30 % younger than those estimated from balloon-borne observations in the middle stratosphere, as demonstrated by Inai (2018). To address this issue, trajectory-based AoA values are uniformly corrected by a correction factor of 1.5 (determined with reference to the AoA obtained from SF_6 mixing ratios) in this study. There is, however, a possibility that the bias differs with the meteorological region, because

30   different mechanisms drive the shallow and deep branches of the BDC (e.g., Birner and Bönisch, 2011). This is a possible cause of the inconsistent relationship between the abundance of N_2O and CH_4 in stratospheric air mass and the mass fraction of the air masses travelling via the deep and shallow branches of the BDC. If the AoA of air masses travelling via the deep branch is assumed to be ~5 years, the relationship approaches those of Andrews et al. (2001) and Röckmann et al. (2011).

Trajectory results also generally depend on the vertical condition, i.e., kinematic (employed by the current study) or diabatic (employed by, for example, Diallo et al., 2017). Previous studies suggest that using kinematic trajectories leads to a stronger dispersion and somewhat young bias in AoA estimates compared with using diabatic trajectories (e.g., Schoeberl et al., 2003; Diallo et al., 2012). Therefore, using diabatic trajectories in this analysis might result in a correction factor (γTT) of <1.5.

5   The second limitation is related to the criteria for the determination of air mass origin. These criteria may strongly affect origin fraction estimates and are thus expected to contribute to the uncertainty of this analysis, to some degree. A comprehensive sensitivity test to address this issue, focusing on in-mixing in the TTL, has been reported by Inai (2018), who found that the mixing fraction can vary by 40 % to 180 %, depending on the choice of criteria. Though the same test could be applied to the current study, the estimated origin fraction distributions are comparable to those estimated based on trace gas observations by

10   the In-service Aircraft for a Global Observing System-Civil Aircraft for the Regular Investigation of the atmosphere Based on an Instrument Container (IAGOS-CARIBIC; Umezawa et al., 2015). Moreover, these estimates are indirectly validated by the CONTRAIL observations, through the reconstruction of the chemical distributions (as evident in Figs 5d and e, and 8). This agreement supports our criteria selection and suggests that our estimated origin fractions are not, at least, grossly wrong. However, the breakdown of stratospheric air masses is subject to the limitations described in the last part of Sect. 4.2. If the

15   relative fraction of air masses travelling via the deep branch is 7 % smaller than the estimated values (i.e., if they were 17 % and 7 % in spring and autumn), the relationship between the abundance of N_2O and CH_4 in stratospheric air mass and the mass fraction of the air masses travelling via the deep and shallow branches also approaches that of Andrews et al. (2001) and Röckmann et al. (2011).

Another limitation may arise from the analysis methodology. The observed mixing ratios of CH_4, N_2O, CO, SF_6, and CO_2 are

20   used after removing linear trends for each time-series, and are considered to be a function of month and treated separately from the long-term trend. This treatment decreases the precision of observations if the observed values have non-linear interannual variations, which is mainly concerned for CO_2. Furthermore, the CONTRAIL measurements were conducted once a month. Thus, one observed value represents atmospheric conditions at a specific spatiotemporal point, whereas the analysis field has a coarser spatiotemporal resolution, corresponding to, at minimum, that of the grid scale of the ERA-Interim dataset. Such a

25   mismatch in spatiotemporal resolution may contribute to the lack of agreement between the reconstructions and CONTRAIL measurements during summer, particularly for CO_2 (Fig. 5e). However, uncertainties arising from these issues are minimized by the use of equivalent latitude and potential temperature, which are dynamically conserved quantities in the stratosphere. In the troposphere, which is more unstable, potential temperature and potential vorticity are not conserved, or are conserved only on much short timescales, because of diabatic motion. It should be noted that tracer uplift from the LT into the UT during

30   summer (particularly for CO_2, as discussed above) cannot be reduced with the coordinate system employed here. Though the current study covers only the ExUTLS over a longitudinal range from 0° E to 140° E for comparison with the CONTRAIL measurements, the origin fractions and reconstructions are trial-evaluated over North America (Appendix A). Results confirm that the origin fractions are consistent between the two regions, and thus support the robustness of the current study. In this study, linear trends for CH_4, N_2O, SF_6, and CO_2 are assumed for the reconstruction. Although this is a simplified treatment,

given the length of the analysis period, these trends are roughly constant over this time period with the exception of CH_4, and the CH_4 reconstructions are more strongly affected by chemical loss, as is evident in a comparison of Figs 5a and 8a. In the reconstruction procedure described in Sect. 2.2.1, it was necessary to assign the average of tropical aircraft and mid-latitude LT measurements to the original values for $k = 2$ to prevent underestimations. As discussed in Sect. 2.2.1, one cause of this underestimation might be subgrid-scale tropospheric upward transport that, although common, cannot be accounted for in the trajectory analysis.

5 Summary

To identify the origin of air masses in the ExUTLS, kinematic backward trajectories were calculated for 10 years following the method of Inai (2018) using ECMWF ERA-Interim data as input. The analysis period extends from January 2012 to December 2016, and trajectories were categorized by origins in the stratosphere, tropical troposphere, mid-latitude LT, and high-latitude LT based on meteorological parameters along each individual trajectory. The origin fractions of air masses originating in each region were estimated as a function of equivalent latitude, potential temperature, and month. Furthermore, using the same trajectory, the mixing fractions of air masses originating via the shallow and deep branches of the BDC were separately estimated along with the AoA.

The origin fractions show obvious seasonal variations. In the mid-equivalent latitude upper ExUTLS, origin fractions of the tropical troposphere exceed 50 % during boreal summer and autumn, whereas origin fractions of the stratosphere via the shallow branch of the BDC are dominant during winter and spring. In the high-equivalent latitude upper ExUTLS, origin fractions of the stratosphere exceed 60 % throughout the year. In the mid- and high-equivalent latitude lower ExUTLS, origin fractions of the mid- and high-latitude troposphere are large during summer, whereas during winter, origin fractions of the tropical troposphere are dominant.

By incorporating the time-series of mixing ratios for several chemical species obtained from ground-based and air-borne observations into the estimated trajectories, the spatiotemporal distributions of the chemical species CH_4, N_2O, CO, SF_6, and CO_2 in the ExUTLS were reconstructed, along with estimations of the original composition of the stratospheric air masses. The reconstructions are calculated to agree with CONTRAIL measurements in the ExUTLS. Furthermore, uniform spatiotemporal species distributions are obtained for the ExUTLS from non-uniform observations. The origin fractions and AoA of each reconstruction are discussed. Distributions of CO and CO_2 are strongly affected by tropospheric air masses because of the short chemical lifetime of the former and large seasonal variations in the troposphere of the latter. In contrast, CH_4, N_2O, and SF_6 distributions are controlled primarily by seasonal variations in air masses transported from the stratosphere and subsequent mixing with tropospheric air masses. This interpretation is qualitatively and quantitatively consistent with the spatiotemporal AoA distributions.

This study developed and demonstrated a unique and effective method to exploit the advantages of observational data in combination with trajectory analysis. This method provides a means to understand both air-mass transport and chemical decay

from a new perspective. Furthermore, this technique can be applied to other data (e.g., species isotope ratios) or analyses of regions where trajectory calculations are effective.

Appendix A. Sensitivity analyses

It is well known that results from trajectory analyses are affected by the resolution of input meteorological data. For example,

5 Inai (2018) suggests that the origin fraction of stratospheric air masses in the upper TTL can vary by ~50 % in magnitude. Here, the sensitivity of our results to data resolution is tested. Figure A1 shows the dependence of origin fractions on the resolution of meteorological data for trajectories launched each month. Note that here, the trajectory calculation length is limited to 90 days due to limited computing resources. Origin fractions calculated from ERA-Interim data and used in this study (1.5° × 1.5° horizontal resolution, 37 vertical levels) are compared with those using a finer resolution (0.75° × 0.75°

10 horizontal resolution, 60 vertical levels). Origin fractions were evaluated for each bin set in an equivalent latitude–potential temperature cross-section (crosses). Results confirm that these points are distributed in a linear fashion with slopes of around 1.0 regardless of season. This suggests that the origin fractions are not quantitatively or qualitatively dependent on the resolution of the input data. This independence differs from the findings of Inai (2018), possibly because transport mechanisms in the ExUTLS are related to synoptic-scale mechanisms rather than convective activity, which dominates the tropical region.

15 In the current study, origin fractions were estimated only for the longitudinal region between 0° E and 140° E, selected for comparison with CONTRAIL measurements over Siberia. Previous studies have investigated mixing processes between tropospheric and stratospheric air masses over different longitudinal regions; e.g., over North America (Pan et al., 2010). To compare our results with these studies, the dependence of origin fraction on longitudinal region was tested. Figure A2 compares origin fractions evaluated over Siberia and North America. Results confirm that the data points in Fig. A2 (crosses) are

20 distributed in a linear fashion with slopes of around 1.0 regardless of season. This suggests that the origin fractions are not quantitatively and qualitatively dependent on longitudinal region. This independence may arise from the employment of equivalent latitude and potential temperature, which are dynamically conserved parameters, in this analysis.

Appendix B. Large-scale perspective of origin fractions and reconstructions

Detailed analyses of origin fractions and reconstructions for specific months are informative, but taking a larger perspective

25 might provide insight into seasonal transport processes and tracer distributions in the ExUTLS. Here, we present a larger-scale perspectives of origin fractions and reconstructions for the ExUTLS. Figure B1 shows monthly origin fractions as a function of time of year. The axes of each panel are as in Figs 10–13. Thus, the seasonal behavior of air-mass transport into the ExUTLS from surrounding areas is visualized. Origin fractions of the stratosphere via both branches of the BDC increase from winter to spring. Subsequently, those via the deep branch become small during summer and autumn. In contrast, origin fractions of

30 the tropical troposphere are prominent during summer and autumn, with the exception of regions of lower potential temperature.

The lower ExUTLS is dominated by air masses originating in the mid-latitude LT throughout the year, but those originating in the high-latitude LT contribute to this lowermost region during summer. The seasonal behavior of reconstructed chemical species is shown in Fig. B2. The patterns of chemically passive tracers, particularly SF_6, follow that of AoA. However, CO_2 in the lower ExUTLS undergoes different seasonal variations. (Note that the CO_2 mixing ratio is likely not well-reconstructed during summer in the lower ExUTLS.) The patterns of CH_4 and N_2O are similar in that the mixing ratios in the deep ExUTLS become small during spring and summer. However, their seasonal transitions slightly differ from each other, which that of CH_4 varies more gradually than another. The mixing ratios of CO in the deep ExUTLS are small throughout the year, but increase slightly during autumn.

Author contribution

Yoichi Inai designed and carried out the study. Toshinobu Machida, Hidekazu Matsueda, Yousuke Sawa, Kazuhiro Tsuboi, and Keiichi Katsumata obtained the measurement data, and Shinji Morimoto, Shuji Aoki, and Takakiyo Nakazawa developed the measurement system. Yoichi Inai and Ryo Fujita prepared the manuscript with contributions from all co-authors.

Acknowledgements

The authors would like to acknowledge the support of many engineers from Japan Airlines and JAMCO Tokyo. All trace gas mixing ratio data at ground-based sites were provided by NOAA/ESRL (National Oceanic and Atmospheric Administration/Earth System Research Laboratory) and were downloaded from the WMO/WDCGG website (https://gaw.kishou.go.jp/). This work was supported by Grants-in-Aid for Scientific Research (18K03738 and 26220101) from the Japan Society for the Promotion of Science and the Arctic Challenge for Sustainability (ArCS) Project by the Ministry of Education, Culture, Sports, Science and Technology, Japan. We thank Masashi Kohma for valuable discussions. We also thank ECMWF for providing the ERA-Interim data. All figures were produced using the GFD-DENNOU Library. The authors sincerely appreciate the constructive comments of two reviewers that greatly improved the manuscript.

References

Andersson, S., Martinsson, B., Vernier, J.-P., Friberg, J., Brenninkmeijer, C., Hermann, M., Velthoven, M., and Zahn, A.: Significant radiative impact of volcanic aerosol in the lowermost stratosphere, Nat. Commun., 6, 7692, doi:10.1038/ncomms8692, 2015.

Andrews, A. E., Boering, K. A., Daube, B. C., Wofsy, S. C., Loewenstein, M., Jost, H., Podolske, J. R., Webster, C. R., Herman, R. L., Scott, D. C., Flesch, G. J., Moyer, E. J., Elkins, J. W., Dutton, G. S., Hurst, D. F., Moore, F. L., Ray, E. A., Romashkin,

P. A., and Strahan, S. E.: Mean ages of stratospheric air derived from in situ observations of CO_2, CH_4, and N_2O, J. Geophys. Res., 106, 32295–32314, doi:10.1029/2001JD000465, 2001.

Appenzeller, C., Holton, J. R., and Rosenlof, K. H.: Seasonal variation of mass transport across the tropopause. J. Geophys. Res. 101, 15071–15078, 1996.

Birner, T., and Bönisch, H.: Residual circulation trajectories and transit times into the extratropical lowermost stratosphere, Atmos. Chem. Phys., 11, 817–827, doi:10.5194/acp-11-817-2011, 2011.

Bönisch, H., Engel, A., Curtius, J., Birner, Th., and Hoor, P.: Quantifying transport into the lowermost stratosphere using simultaneous in-situ measurements of SF_6 and CO_2, Atmos. Chem. Phys., 9, 5905-5919, https://doi.org/10.5194/acp-9-5905-2009, 2009.

Boothe, A. C. and Homeyer C. R.: Global large-scale stratosphere-troposphere exchange in modern reanalyses, Atmos. Chem. Phys., 17, 5537-5559, doi:10.5194/acp-17-5537-2017, 2017.

Brewer, A. W.: Evidence for a world circulation provided by the measurements of helium and water vapour distribution in the stratosphere, Q. J. Roy. Meteor. Soc., 75, 351–363, doi:10.1002/qj.49707532603, 1949.

Dee, D. P., Uppala, S. M., Simmons, A. J., Berrisford, P., Poli, P., Kobayashi, S., et al.: The ERA-Interim reanalysis: Configuration and performance of the data assimilation system. Quarterly Journal of the Royal Meteorological Society, 137(656), 553–597. https://doi.org/10.1002/qj.828, 2011.

Diallo, M., Legras, B., and Chédin, A.: Age of stratospheric air in the ERA-Interim, Atmos. Chem. Phys., 12, 12133-12154, https://doi.org/10.5194/acp-12-12133-2012, 2012.

Diallo, M., Legras, B., Ray, E., Engel, A. and Añel, J. A.: Global distribution of CO2 in the upper troposphere and stratosphere, Atmos. Chem. Phys., 17(6), 3861-3878, doi:10.5194/acp-17-3861-2017, 2017.

Dlugokencky, E. J., Crotwell, A. M., Lang, P. M., Mund, J. W., and, Rhodes, M. E.: Atmospheric Methane Dry Air Mole Fractions from quasi-continuous measurements at Barrow, Alaska and Mauna Loa, Hawaii, 1986-2017, Version: 2018-03-19, Path: ftp://aftp.cmdl.noaa.gov/data/trace_gases/ch4/in-situ/surface/, 2018a.

Dlugokencky, E. J., Lang, P. M., Crotwell, A. M., Mund, J. W., Crotwell, M. J., and Thoning, K. W.: Atmospheric Methane Dry Air Mole Fractions from the NOAA ESRL Carbon Cycle Cooperative Global Air Sampling Network, 1983-2017, Version: 2018-08-01, Path: ftp://aftp.cmdl.noaa.gov/data/trace_gases/ch4/flask/surface/, 2018b.

5   Dlugokencky, E. J., Lang, P. M., Mund, J. W., Crotwell, A. M., Crotwell, M. J., and Thoning, K. W.: Atmospheric Carbon Dioxide Dry Air Mole Fractions from the NOAA ESRL Carbon Cycle Cooperative Global Air Sampling Network, 1968-2017, Version: 2018-07-31, Path: ftp://aftp.cmdl.noaa.gov/data/trace_gases/co2/flask/surface/, 2018c.

Dobson, G. M. B.: Origin and Distribution of the Polyatomic Molecules in the Atmosphere, P. Roy. Soc. Lond. A. Mat., 236, 10   187–193, 1956.

Dutton, G., Elkins, J. II, Hall, B., and NOAA ESRL: Earth System Research Laboratory Halocarbons and Other Atmospheric Trace Gases Chromatograph for Atmospheric Trace Species (CATS) Measurements, Version 1. NOAA National Centers for Environmental Information. doi:10.7289/V5X0659V, 2017.

Engel, A., Strunk, M., Muller, M., Haase, H. P., Poss, C., Levin, I., and Schmidt, U.: Temporal development of total chlorine in the high-latitude stratosphere based on reference distributions of mean age derived from CO_2 and SF_6, J. Geophys. Res., 107(D12), doi:Artn 4136, Doi 10.1029/2001jd000584, 2002.

20   Gettelman, A., Hoor, P., Pan, L. L., Randel, W. J., Hegglin, M. I., and Birner, T.: The extratropical upper troposphere and lower stratosphere, Rev. Geophys., 49, RG3003, doi:10.1029/2011RG000355, 2011.

Hall, T. M., and Plumb, R. A.: Age as a Diagnostic of Stratospheric Transport, J. Geophys. Res., 99(D1), 1059-1070, 1994.

25   Holton, J. R. et al.: Stratosphere-troposphere exchange, Rev. Geophys., 33, 403-440, 1995.

Hoor, P., Gurk, C., Brunner, D., Hegglin, M. I., Wernli, H., and Fischer, H.: Seasonality and extent of extratropical TST derived from in-situ CO measurements during SPURT, Atmos. Chem. Phys., 4, 1427-1442, 2004.

30   Inai, Y.: Long-term variation in the mixing fraction of tropospheric and stratospheric air masses in the upper tropical tropopause layer. Journal of Geophysical Research: Atmospheres, 123, https://doi.org/10.1029/2018JD028300, 2018.

Ishijima, K., Nakazawa, T., Sugawara, S., Aoki, S., and Saeki, T.: Concentration variations of tropospheric nitrous oxide over Japan, Geophys. Res. Lett., 28, 171–174, doi:10.1029/2000GL011465, doi:10.1029/2000GL011465, 2001.

Krause, J., Hoor, P., Engel, A., Plöger, F., Grooß, J.-U., Bönisch, H., Keber, T., Sinnhuber, B.-M., Woiwode, W., and Oelhaf, H.: Mixing and ageing in the polar lower stratosphere in winter 2015–2016, Atmos. Chem. Phys., 18, 6057-6073, https://doi.org/10.5194/acp-18-6057-2018, 2018.

Lin, P., Ming, Y. and Ramaswamy, V.: Tropical climate change control of the lower stratospheric circulation, Geophys. Res. Lett., 42, 941–948, doi:10.1002/2014GL062823, 2015.

Manney, G. L., et al.: Jet characterization in the upper troposphere/lower stratosphere (UTLS): Applications to climatology and transport studies, Atmos. Chem. Phys., 11, 6115-6137, 2011.

Machida, T., Matsueda, H., Sawa, Y., Nakagawa, Y., Hirotani, K., Kondo, N., Goto, K., Nakazawa, T., Ishikawa, K., and Ogawa, T.: Worldwide measurements of atmospheric CO_2 and other trace gas species using commercial airlines, J. Atmos. Oceanic Technol., 25(10), 1744–1754, doi:10.1175/2008JTECHA1082.1, 2008.

Matsueda, H., and Inoue, H. Y., Measurements of atmospheric CO_2 and CH_4 using a commercial airliner from 1993 to 1994, Atmos. Environ., 30, 1647–1655, 1996.

Matsueda, H., Inoue, H. Y., and Ishii, M.: Aircraft observation of carbon dioxide at 8–13 km altitude over the western Pacific from1993 to 1999, Tellus Ser. B, 54, 1–21, 2002.

Nakazawa, T., Morimoto, S., Aoki, S., and Tanaka, M.: Time and space variations of the carbon isotopic ratio of tropospheric carbon dioxide over Japan, Tellus B, 45, 258–274, 1993.

25 Pan, L. L., Bowman, K. P., Atlas, E. L., Wofsy, S. C., Zhang, F., Bresch, J. F., Ridley, B. A., Pittman, J. V., Homeyer, C. R., Romashkin, P. A., and Cooper, W. A.: The Stratosphere–Troposphere Analyses of Regional Transport 2008 Experiment, B. Am. Meteorol. Soc., 91, 327–342, https://doi.org/10.1175/2009BAMS2865.1, 2010.

Pan, L. L., Honomichl, S. B., Kinnison, D. E., Abalos, M., Randel, W. J., Bergman, J. W., and Bian, J.: Transport of chemical tracers from the boundary layer to stratosphere associated with the dynamics of the Asian summer monsoon, J. Geophys. Res., 121, 14159–14174, https://doi.org/10.1002/2016JD025616, 2016.

Petron, G., Crotwell, A.M., Lang, P. M., and Dlugokencky, E.: Atmospheric Carbon Monoxide Dry Air Mole Fractions from the NOAA ESRL Carbon Cycle Cooperative Global Air Sampling Network, 1988-2017, Version: 2018-10-17, Path: ftp://aftp.cmdl.noaa.gov/data/trace_gases/co/flask/surface/, 2018.

Ploeger, F., and Birner T.: Seasonal and inter-annual variability of lower stratospheric age of air spectra, Atmos. Chem. Phys., 16(15), 10195-10213, doi:10.5194/acp-16-10195-2016, 2016.

Ploeger, F., Konopka, P., Walker, K., and Riese, M.: Quantifying pollution transport from the Asian monsoon anticyclone into the lower stratosphere, Atmos. Chem. Phys., 17, 7055-7066, https://doi.org/10.5194/acp-17-7055-2017, 2017.

Plumb, R. A., Tracer interrelationships in the stratosphere, Rev. Geophys., 45(4), Artn Rg4005, doi:10.1029/2005rg000179, 2007.

Randel, W. J. and Park, M.: Deep convective influence on the Asian summer monsoon anticyclone and associated tracer variability observed with Atmospheric Infrared Sounder (AIRS), J. Geophys. Res., 111, D12314, doi:10.1029/2005JD006490, 2006.

Randel, W. J., Park, M., Emmons, L., Kinnison, D., Bernath, P., Walker, K. A., Boone, C., and Pumphrey, H.: Asian Monsoon Transport of Pollution to the Stratosphere, Science, 328, 611– 613, doi:10.1126/science.1182274, 2010.

Röckmann, T., Brass, M., Borchers, R., and Engel, A.: The isotopic composition of methane in the stratosphere: high-altitude balloon sample measurements, Atmos. Chem. Phys., 11, 13287-13304, https://doi.org/10.5194/acp-11-13287-2011, 2011.

Sawa, Y., Machida, T., Matsueda, H., Niwa, Y., Tsuboi, K., Murayama, S., Morimoto, S., and Aoki, S.: Seasonal changes of CO_2, CH_4, N_2O, and SF_6 in the upper troposphere/lower stratosphere over the Eurasian continent observed by commercial airliner, Geophys. Res. Lett., 42, 2001–2008, doi:10.1002/2014GL062734, 2015.

Schoeberl, M. R., Sparling, L. C., Jackman, C. H., and Fleming, E. L.: A Lagrangian view of stratospheric trace gas distributions, Journal of Geophysical Research: Atmospheres, 105(D1), 1537-1552, doi:10.1029/1999JD900787, 2000.

Schoeberl, M. R., Douglass, A. R., Zhu, Z., and Pawson, S.: A comparison of the lower stratospheric age spectra derived from a general circulation model and two data assimilation systems. Journal of Geophysical Research, 108(D3), 4113. https://doi.org/10.1029/2002JD002652, 2003.

Strahan, S. E., Duncan, B. N., and Hoor, P.: Observationally derived transport diagnostics for the lowermost stratosphere and their application to the GMI chemistry and transport model, Atmos. Chem. Phys., 7, 2435-2445, https://doi.org/10.5194/acp-7-2435-2007, 2007.

5   Thoning, K. W., Kitzis, D. R., and Crotwell, A.: Atmospheric carbon dioxide dry air mole fractions from quasi-continuous measurements at Barrow, Alaska, Version: 2018-10, Path: http://dx.doi.org/10.7289/V5RR1W6B, 2017.

Umezawa, T., Goto, D., Aoki, S., Ishijima, K., Patra, P. K., Sugawara, S., Morimoto, S., and Nakazawa, T.: Variations of tropospheric methane over Japan during 1988–2010, Tellus B, 66, 23837, doi:10.3402/tellusb.v66.23837, 2014.

Umezawa, T., Baker, A. K., Brenninkmeijer, C. A. M., Zahn, A., Oram, D. E., and van Velthoven, P. F. J.: Methyl chloride as a tracer of tropical tropospheric air in the lowermost stratosphere inferred from IAGOS-CARIBIC passenger aircraft measurements, J. Geophys. Res., 120, 12313–12326, doi:10.1002/2015JD023729, 2015.

15   Vogel, B., et al.: Long-range transport pathways of tropospheric source gases originating in Asia into the northern lower stratosphere during the Asian monsoon season 2012, Atmos. Chem. Phys., 16, 15301-15325, https://doi.org/10.5194/acp-16-15301-2016, 2016.

Volk, C. M., Elkins, J. W., Fahey, D. W., Dutton, G. S., Gilligan, J. M., Loewenstein, M., Podolske, J. R., Chan, K. R., and
20   Gunson, M. R.: Evaluation of source gas lifetimes from Stratospheric observations, J. Geophys. Res., 102(D21), 25 543– 25 564, doi:10.1029/97JD02215, 1997.

Wernli, H., and Bourqui, M.: A Lagrangian ''1-year climatology'' of (deep) cross-tropopause exchange in the extratropical Northern Hemisphere, J. Geophys. Res., 107(D2), 4021, doi:10.1029/2001JD000812, 2002.

Table 1: Criteria for determining air mass origin. Each trajectory is categorized once it continuously satisfies one set of criteria k = 1, 2, 3, or 4 during three continuous days along its path.

Category #	Origin	Criteria
k = 1d	Deep stratosphere	Pot. temperature >400 K; P <30 hPa within 4 years
k = 1s	Shallow stratosphere	Pot. temperature >400 K; not satisfied k = 1d
k = 2	Tropical troposphere	Pot. temperature <350 K; lat. <20° N; pot. vorticity <1 PVU
k = 3	Mid-latitude LT	Z <4 km; 20° N < lat. <45° N
k = 4	High-latitude LT	Z <4 km; lat. >45° N
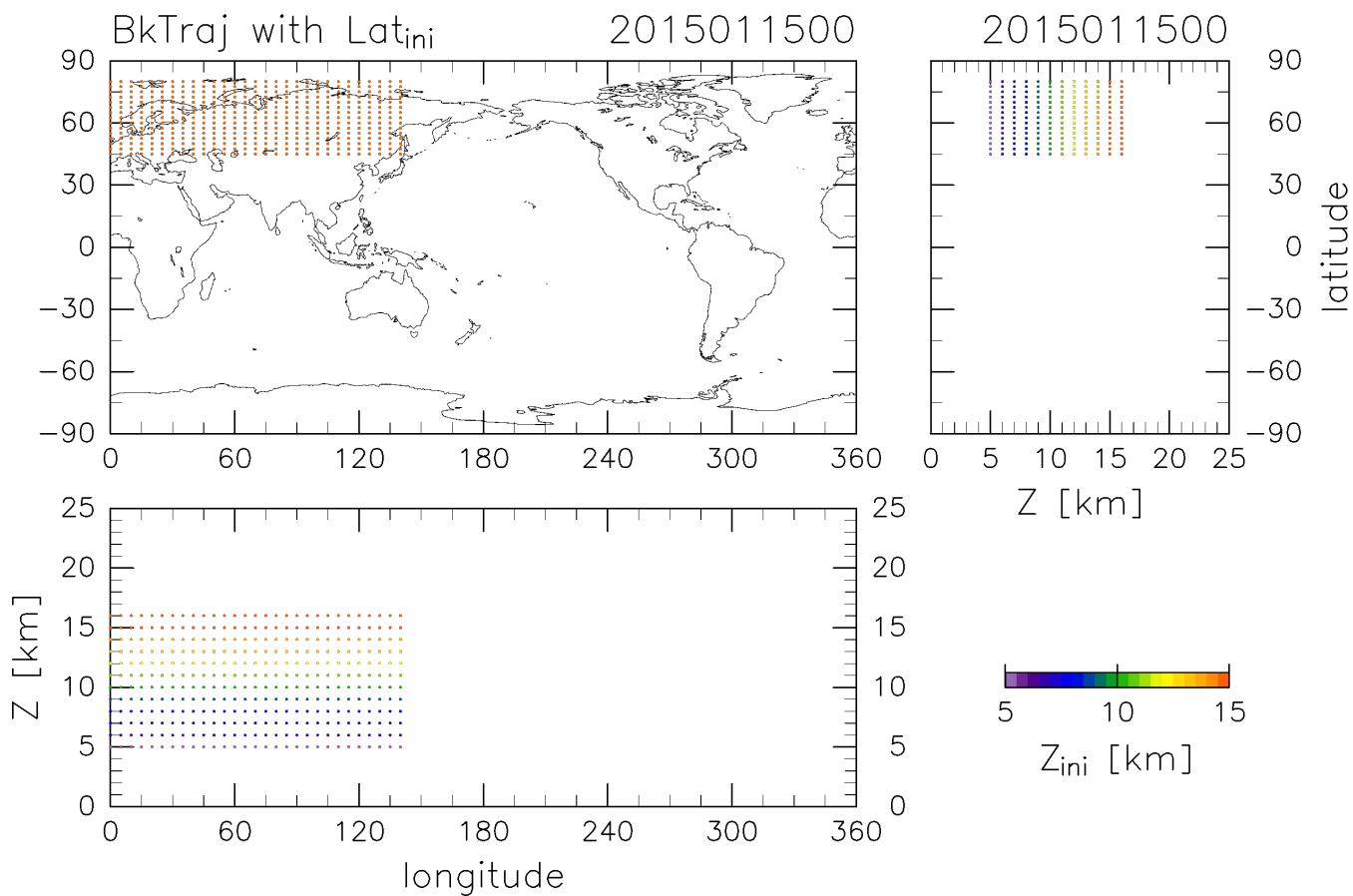
Figure 1: Initial trajectory positions projected in (top-left) longitude–latitude, (top-right) height–latitude, and (bottom) longitude–height sections. Colours indicate the initial height for each position.
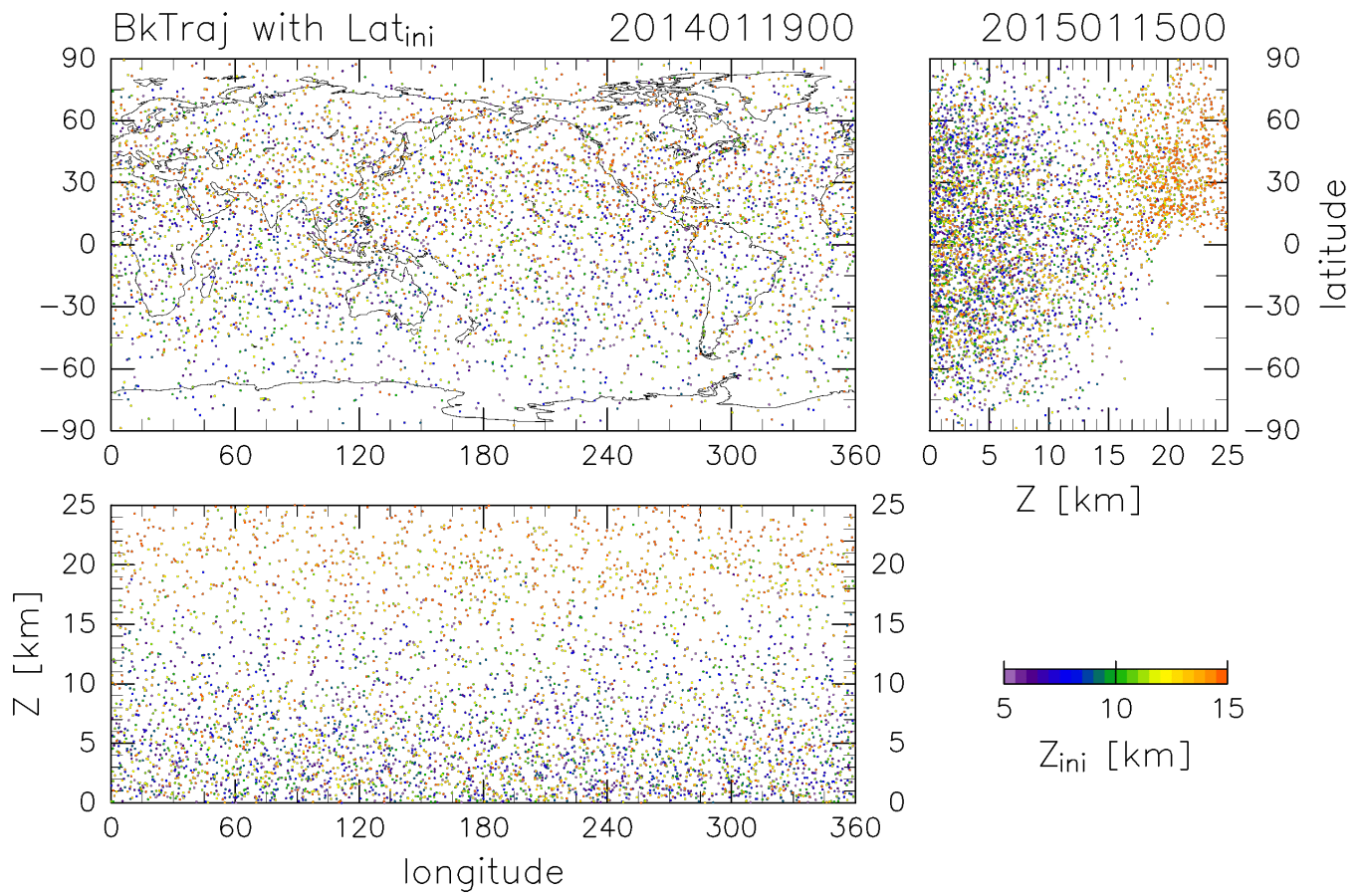
Figure 2: As in Fig. 1, but for the terminal positions of trajectories after calculating backward for 361 days.
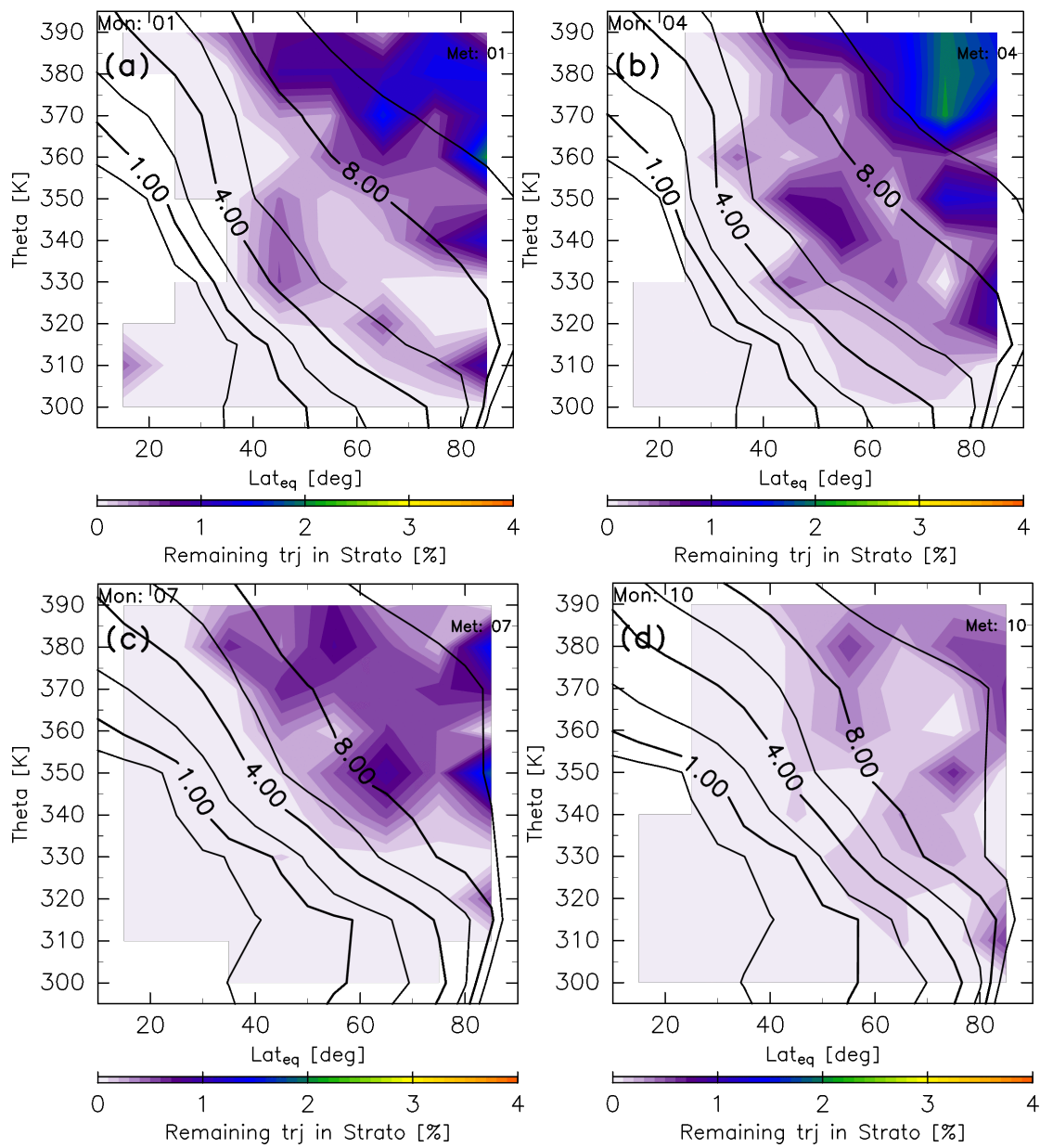
Figure 3: Meridional distributions of percentage of trajectories that remain in the stratosphere after 10-year backward calculations for (a) January, (b) April, (c) July, and (d) October. Black contours indicate monthly average potential vorticity during 2012–2016.
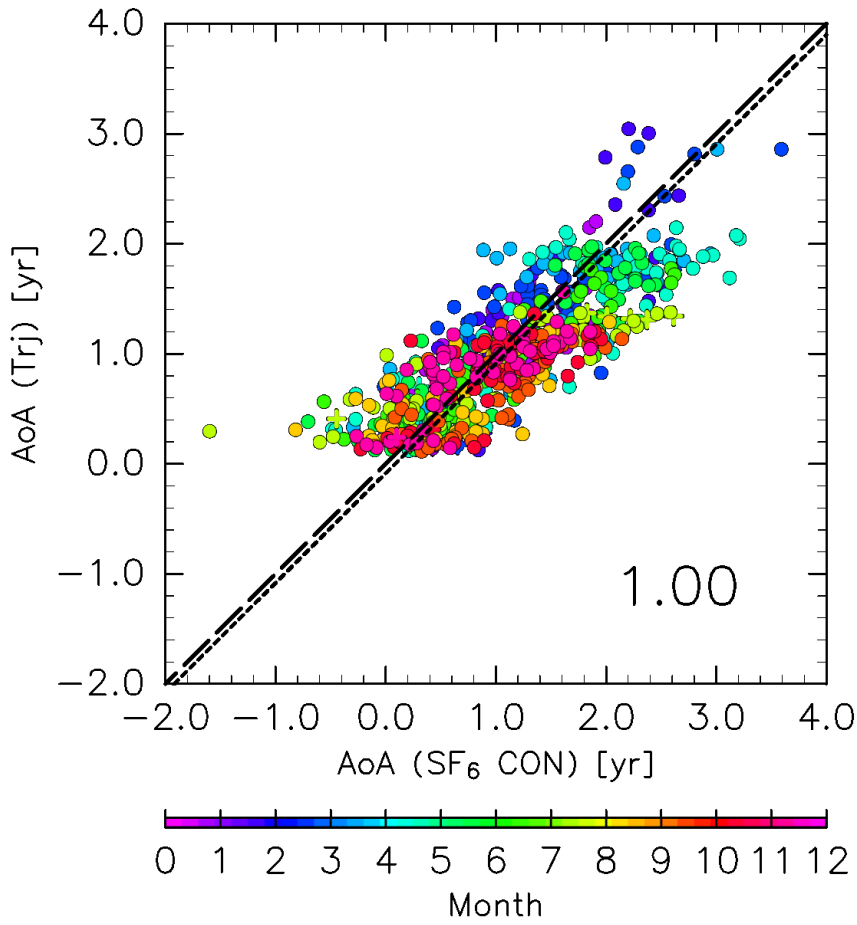
Figure 4: Scatter plot of the age of air (AoA) estimated from SF$_6$ mixing ratios obtained from CONTRAIL measurements versus those from trajectories with a correction factor of 1.5 (see text for details). Colours indicate the month, and the dashed and dotted lines indicate the 1:1 line and the regression line, respectively. The number in the lower-right of the panel indicates the slope of the regression line. CONTRAIL data with CO mixing ratios higher than 80 ppb in the region above 340 K and north of 60° N equivalent latitude are plotted in crosses.
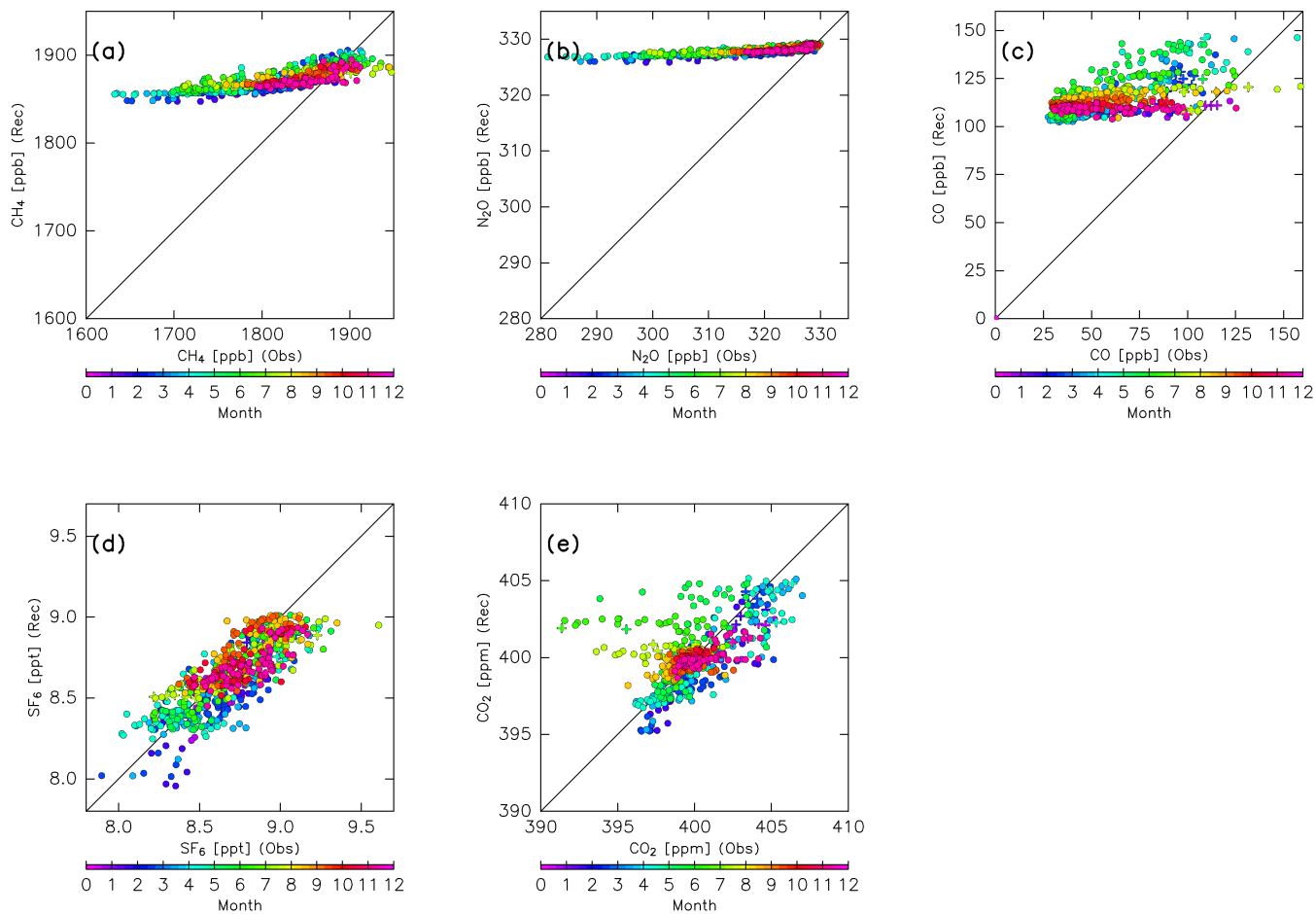
Figure 5: Scatter plots of CONTRAIL measurements versus reconstructions for (a) CH$_4$, (b) N$_2$O, (c) CO, (d) SF$_6$, and (e) CO$_2$ without chemical loss. Colours indicate the month.
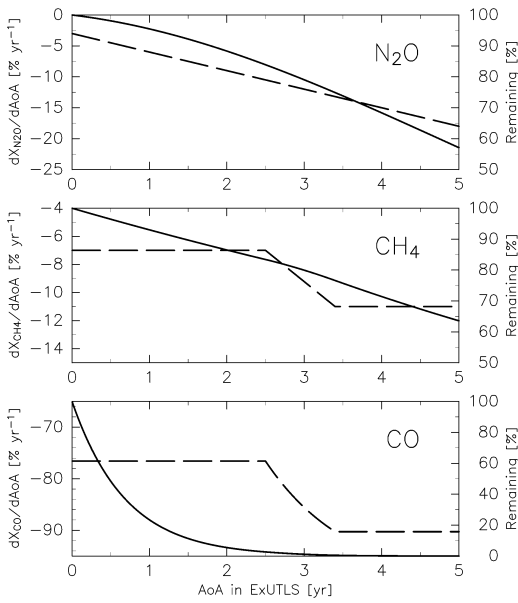
Figure 6: Relationships between the age of air (AoA) and the gradient of chemical loss rates (dashed lines; left axis) and relative abundance (solid lines; right axis), determined according to figure 6a of Volk et al. (1997). Note that CO is assumed to be 20-times the CH₄ value.
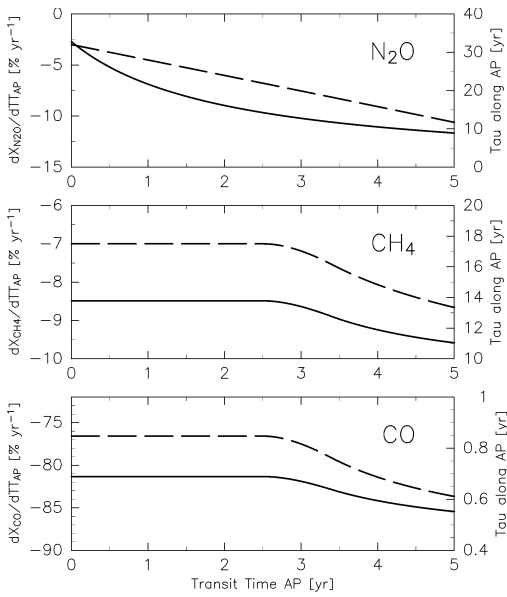
Figure 7: Relationships between transit time along the "average path" (AP) and the gradient of chemical loss rate with respect to transit time that produces the same relationship between age of air (AoA) and the gradient of chemical loss rate shown in Fig. 6 (dashed lines; left axis; see text for details), and e-folding times corresponding to chemical loss rates along an AP (solid lines; right axis).
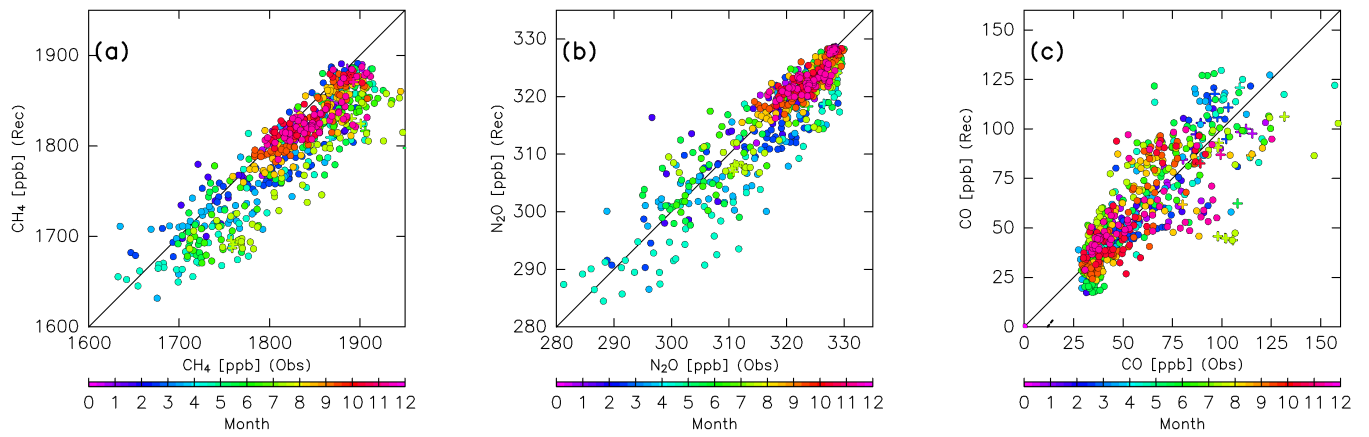
Figure 8: As in Fig. 6, but for reconstructions with chemical loss.
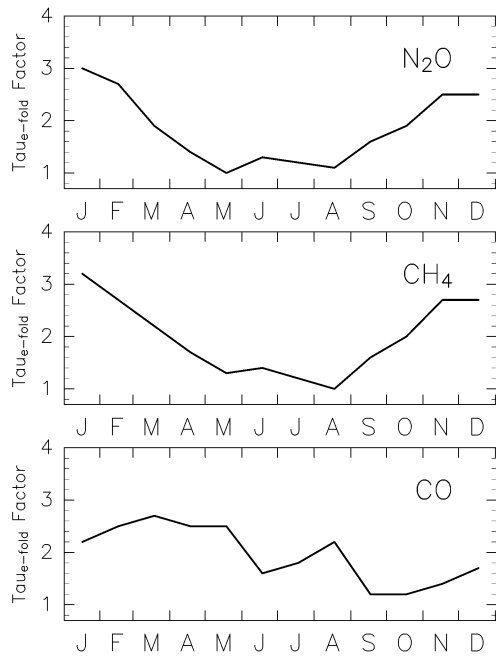
Figure 9: Estimated correction factor for e-folding times for three chemically active species.
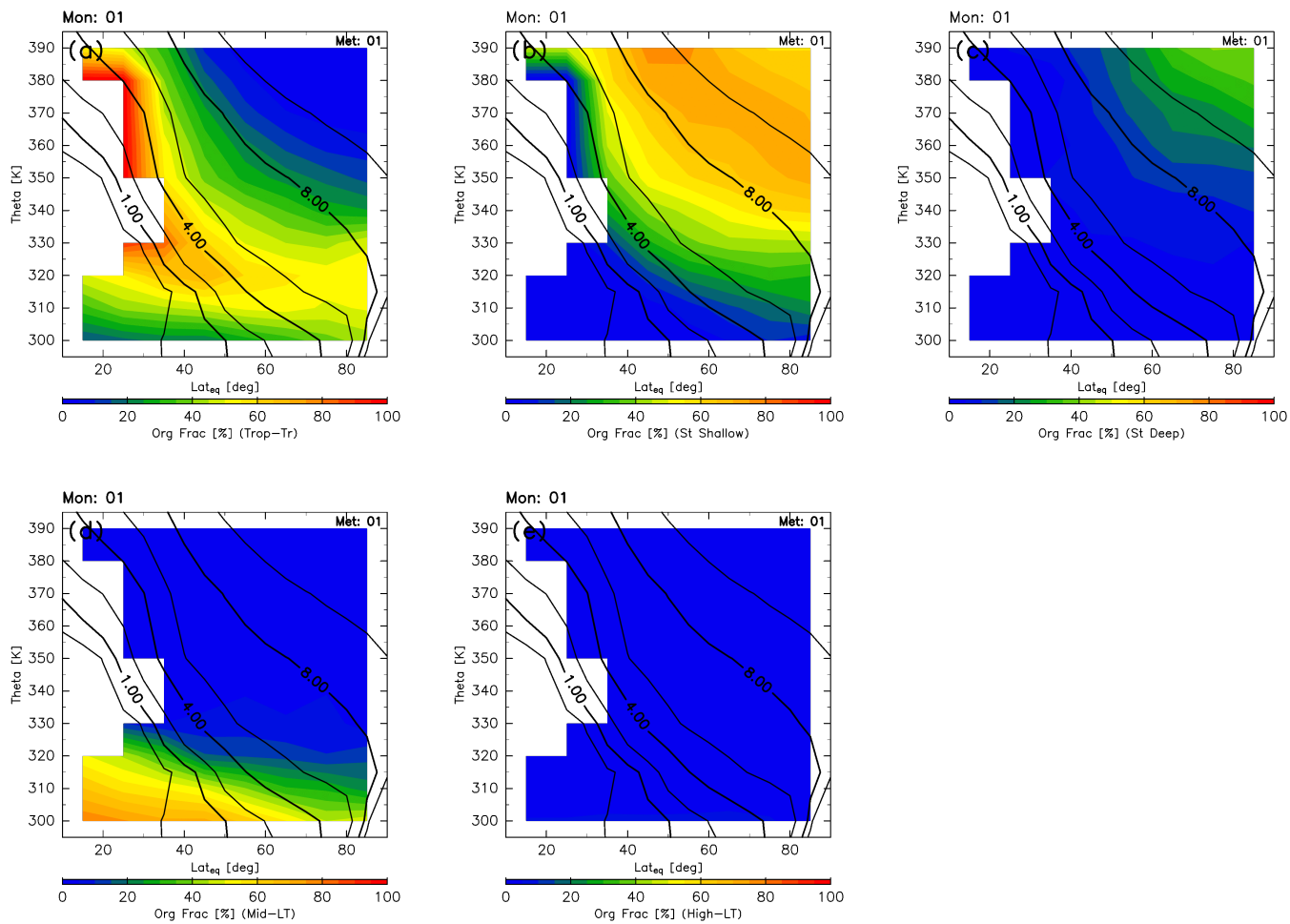
Figure 10: Meridional distributions of origin fractions for (a) tropical tropospheric, (b) stratospheric (through the shallow branch of the BDC), (c) stratospheric (through the deep branch of the BDC), (d) mid-latitude LT, and (e) high-latitude LT air masses estimated for January. Black contours indicate monthly averaged potential vorticity during the period from 2012 to 2016.
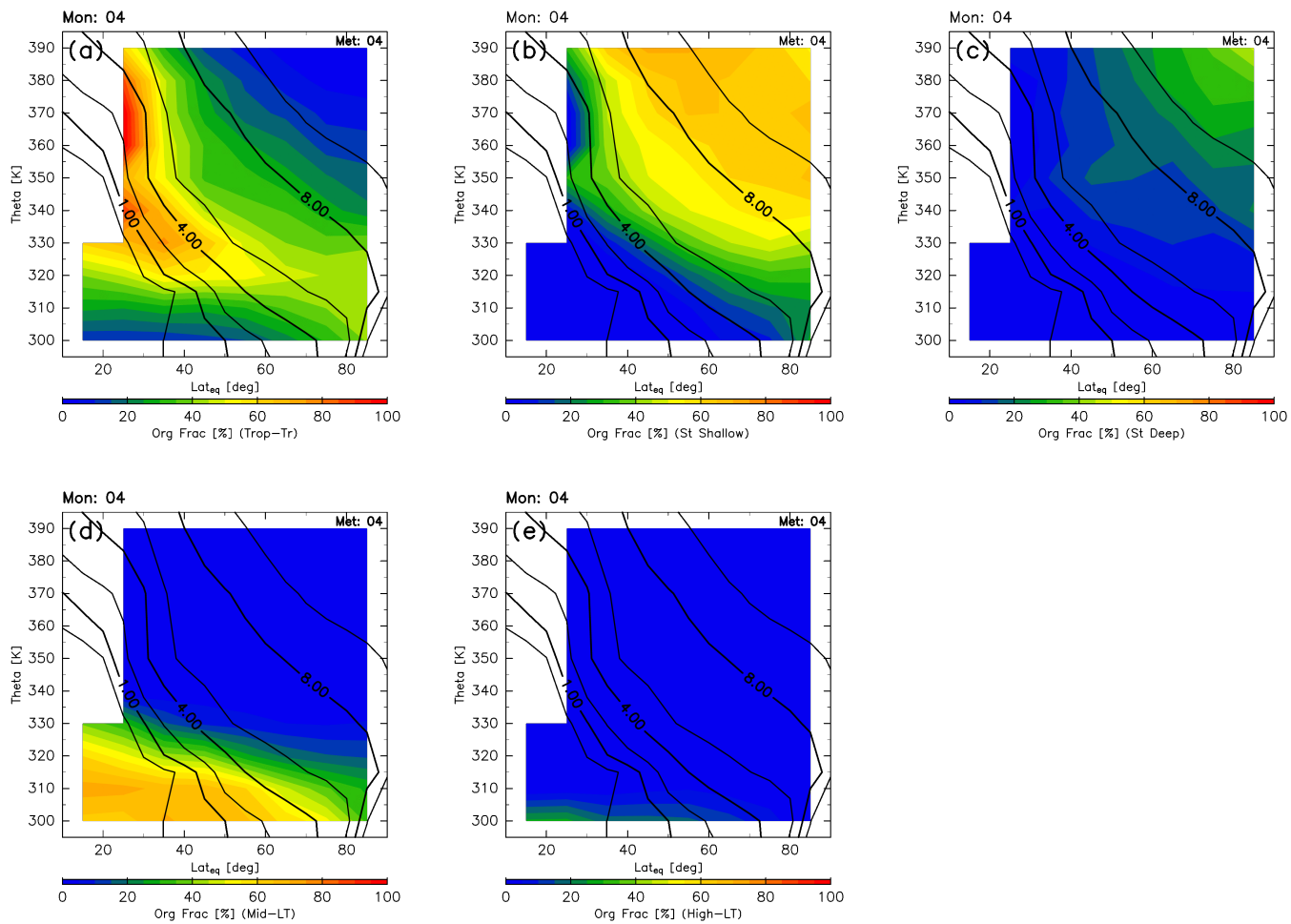
Figure 11: As in Fig. 10, but for April.
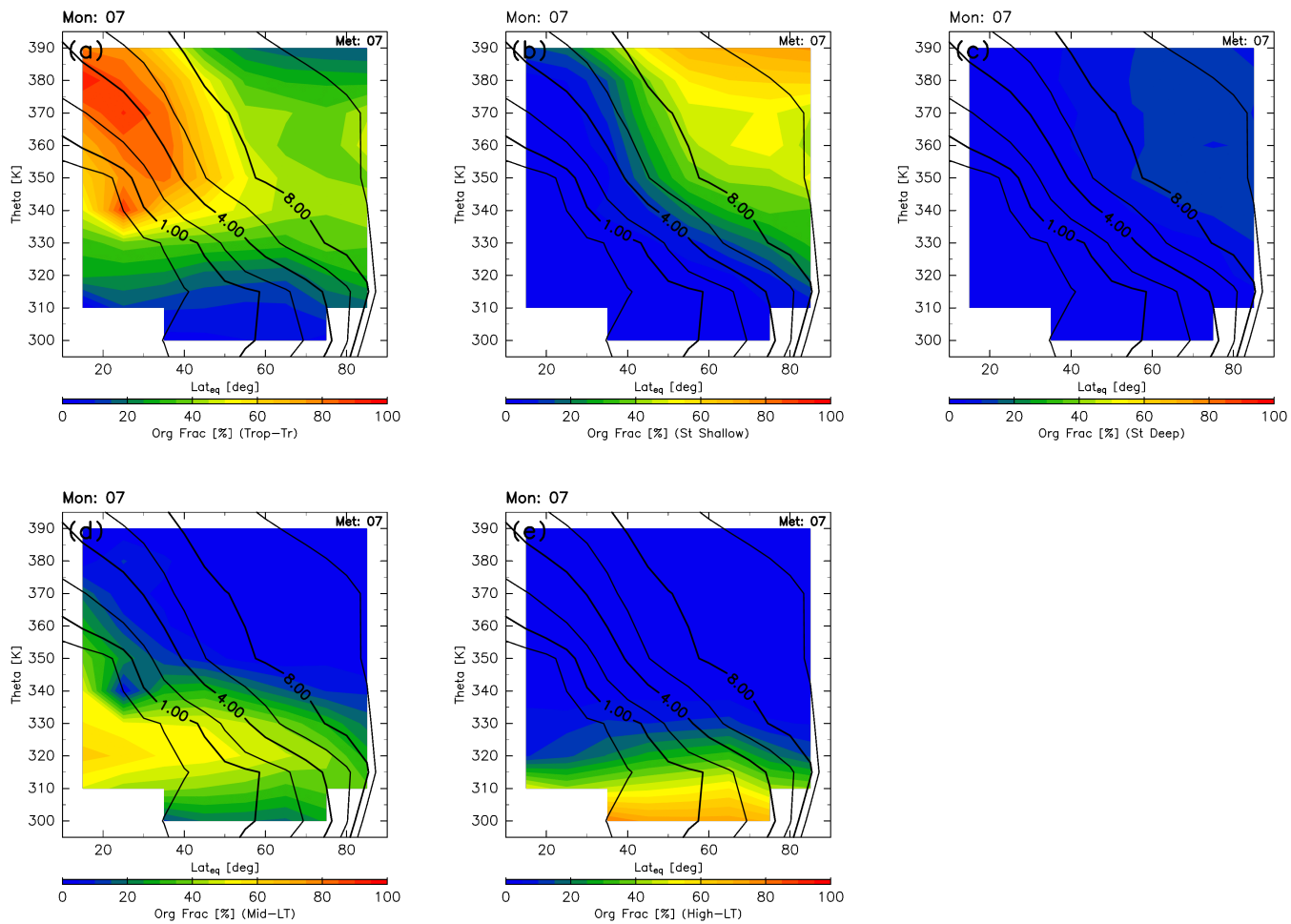
Figure 12: As in Fig. 10, but for July.
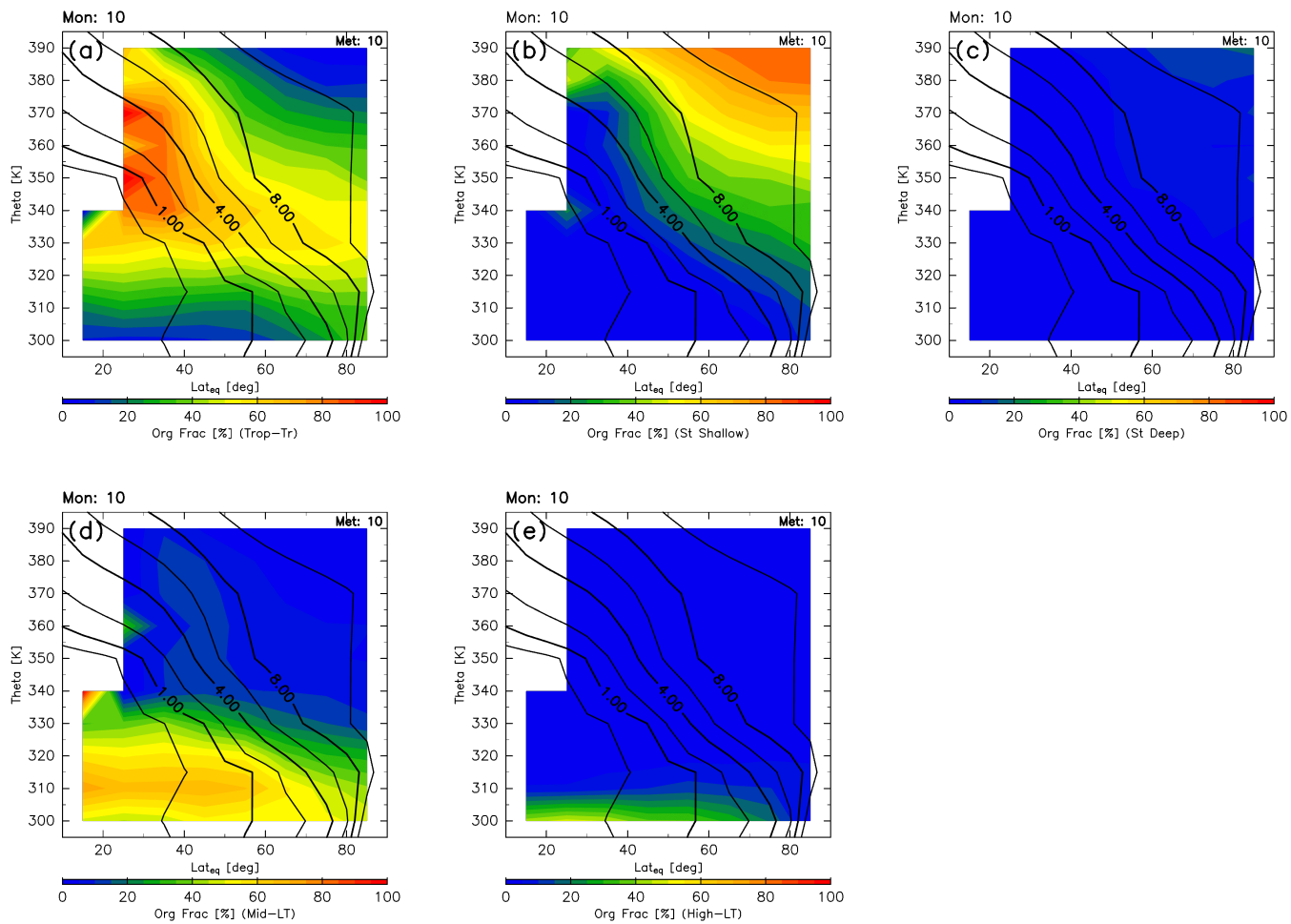
Figure 13: As in Fig. 10, but for October.
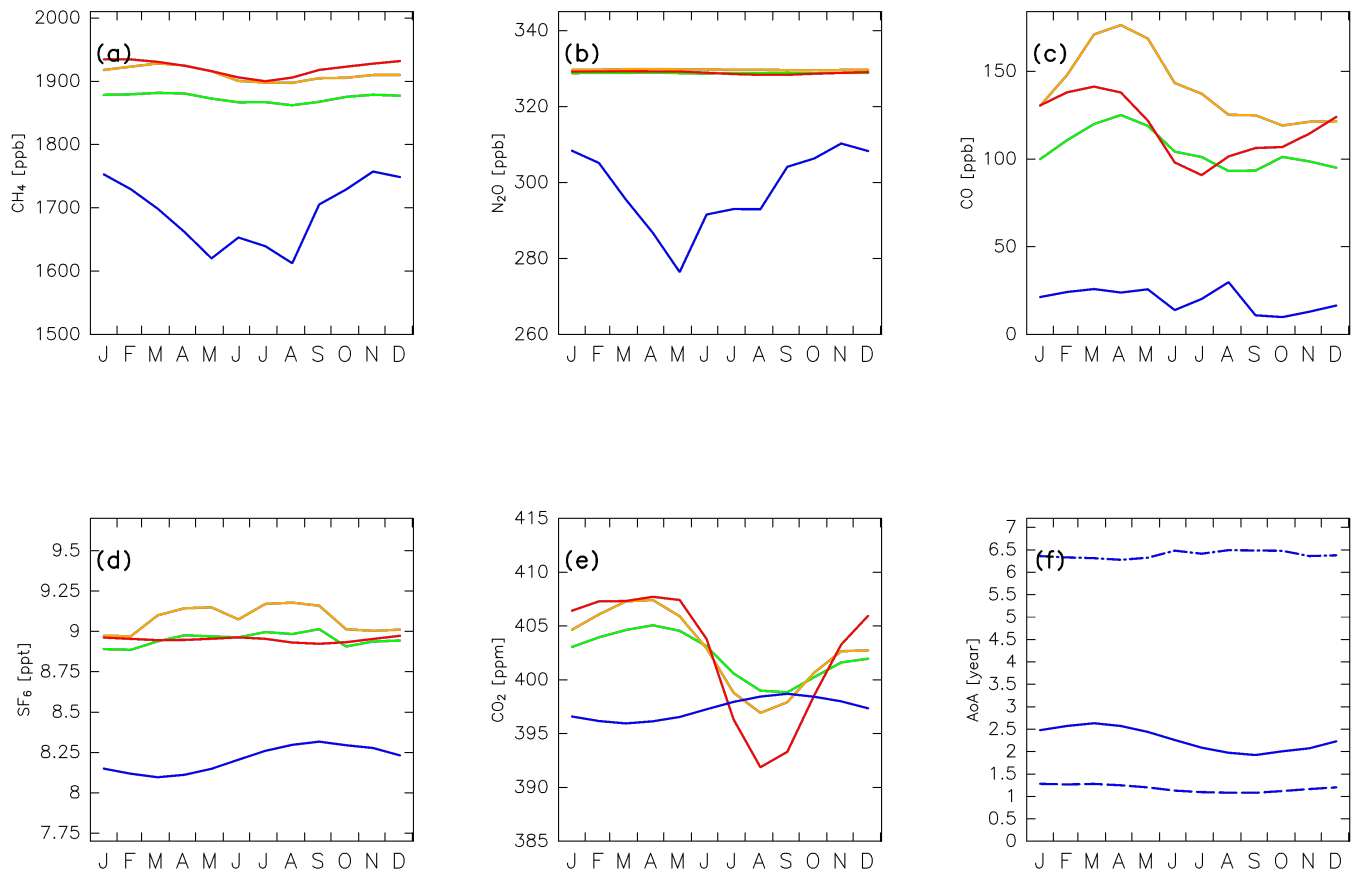
Figure 14: Seasonal variations in (a) CH$_4$, (b) N$_2$O, (c) CO, (d) SF$_6$, and (e) CO$_2$ mixing ratios assigned to (green) tropical tropospheric, (orange) mid-latitude LT, and (red) high-latitude LT air masses. Blue lines in (a–e) show the mixing ratios of each species estimated for stratospheric air masses (see text for details). Seasonal variations in the age of air (AoA) estimated for (blue solid lines) stratospheric air masses are shown in (f). Dashed–dotted and dashed lines in (f) indicate the AoA separately estimated for stratospheric air masses that travelled via the deep and shallow branches of the BDC, respectively.
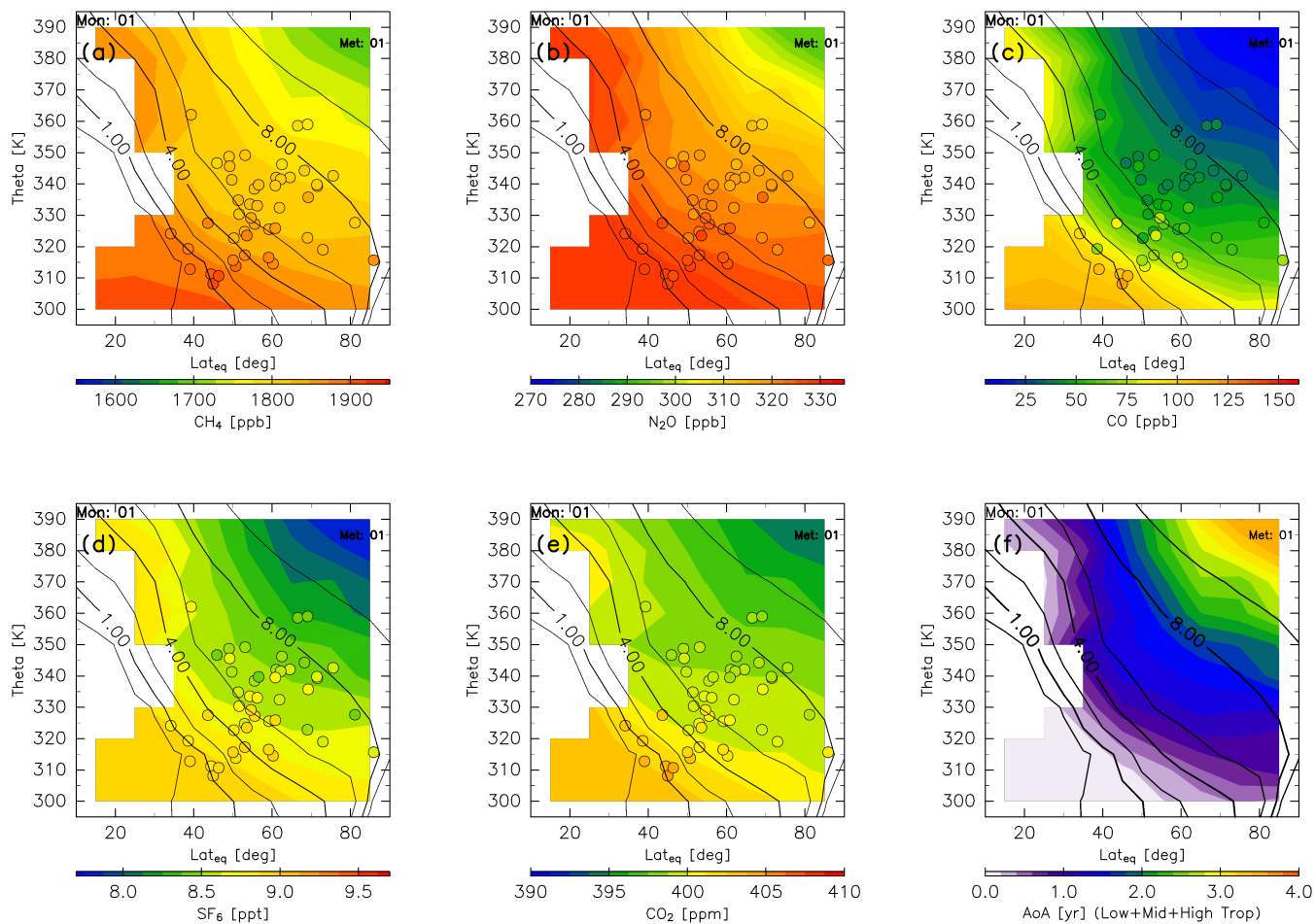
Figure 15: Meridional distributions of reconstructions for (a) CH₄, (b) N₂O, (c) CO, (d) SF₆, and (e) CO₂ for January. Detrended CONTRAIL measurements in January are plotted as circles using the same colour scale. The distribution of the age of air (AoA) estimated for January is shown in (f). Black contours indicate monthly average potential vorticity during the period from 2012 to 2016.
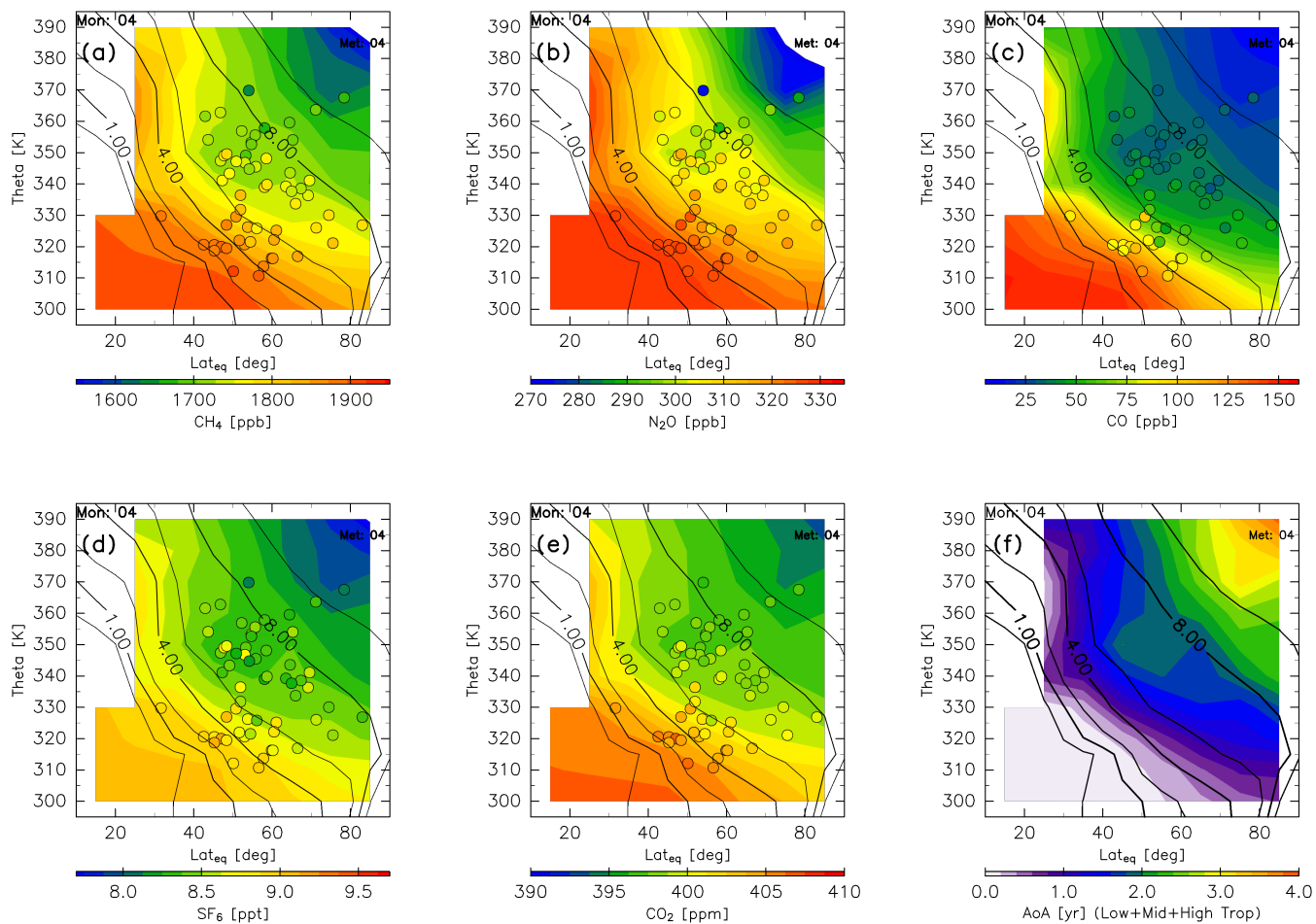
Figure 16: As in Fig. 8, but for April.
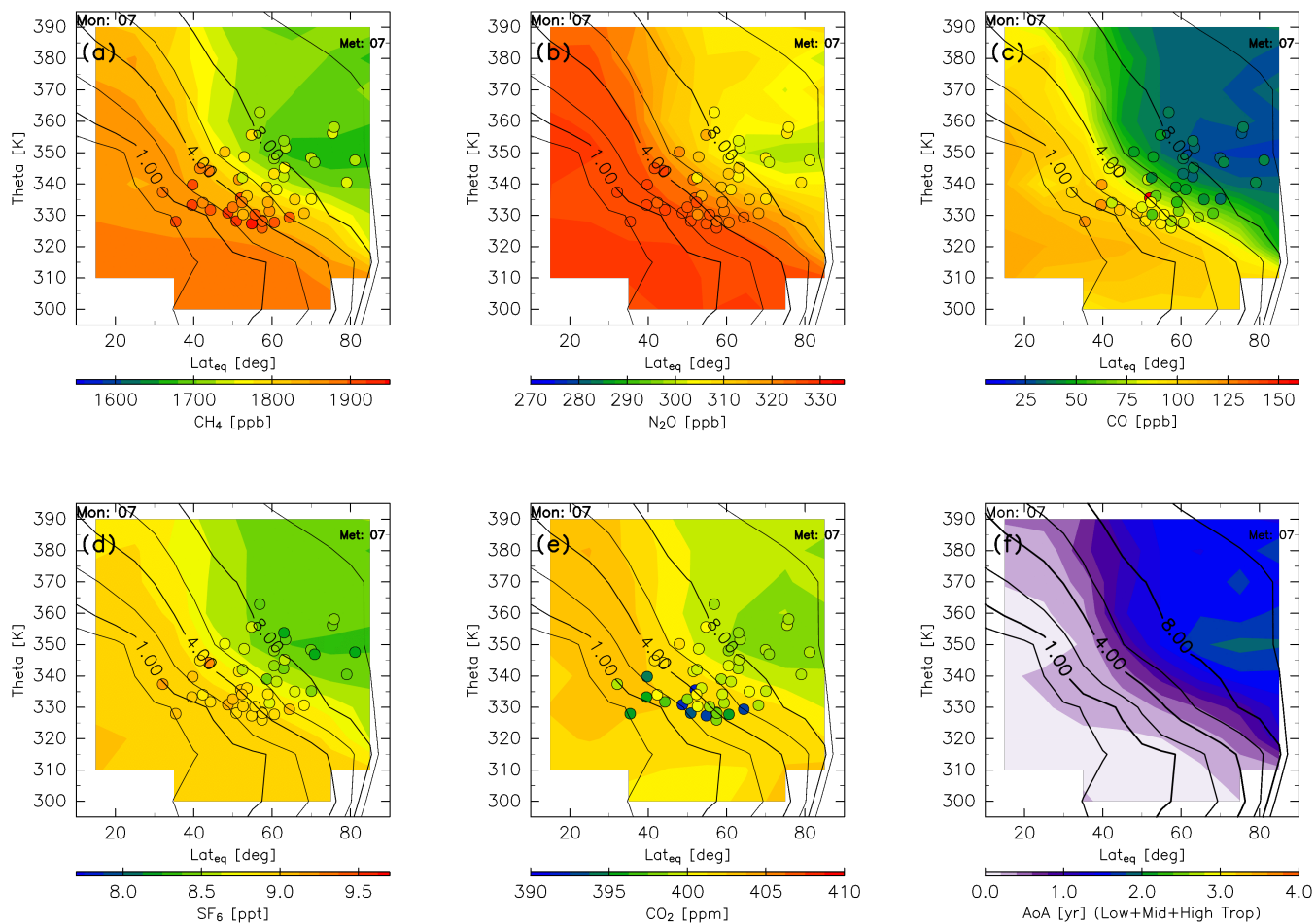
Figure 17: As in Fig. 8, but for July.
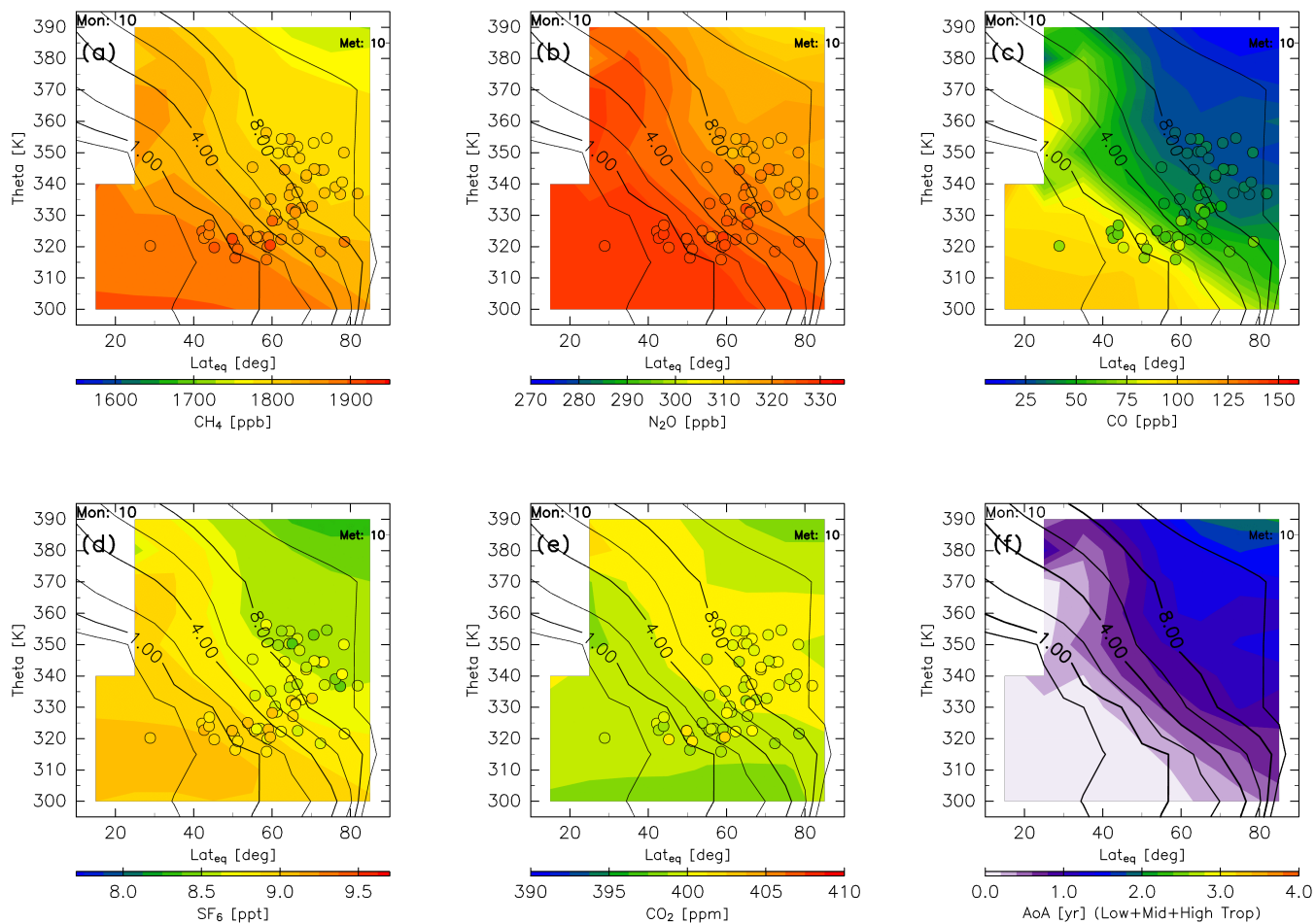
Figure 18: As in Fig. 8, but for October.
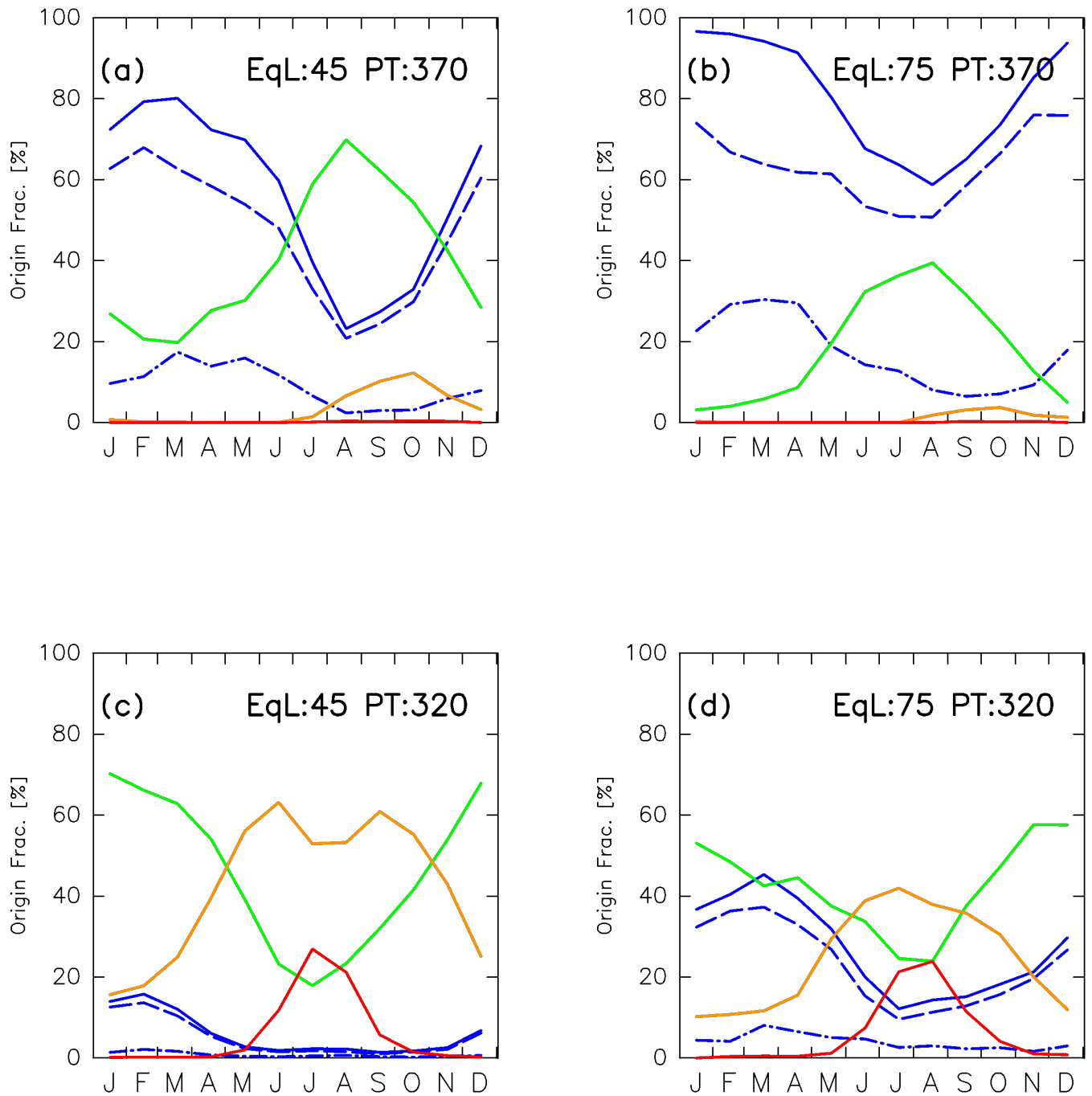
Figure 19: Seasonal variations in (green) tropical tropospheric, (blue) stratospheric, (orange) mid-latitude LT, and (red) high-latitude LT origin fractions estimated for the (a) mid-latitude upper ($\emptyset_{eq} = 45°N$; $\theta = 370$ K), (b) high-latitude upper ($\emptyset_{eq} = 75°N$; $\theta = 370$ K), (c) mid-latitude lower ($\emptyset_{eq} = 45°N$; $\theta = 320$ K), and (d) high-latitude lower ($\emptyset_{eq} = 75°N$; $\theta = 320$ K) ExUTLS. The blue dashed–dotted and dashed lines show the origin fractions of stratospheric air masses that travelled through the deep and shallow branches of the BDC, respectively.
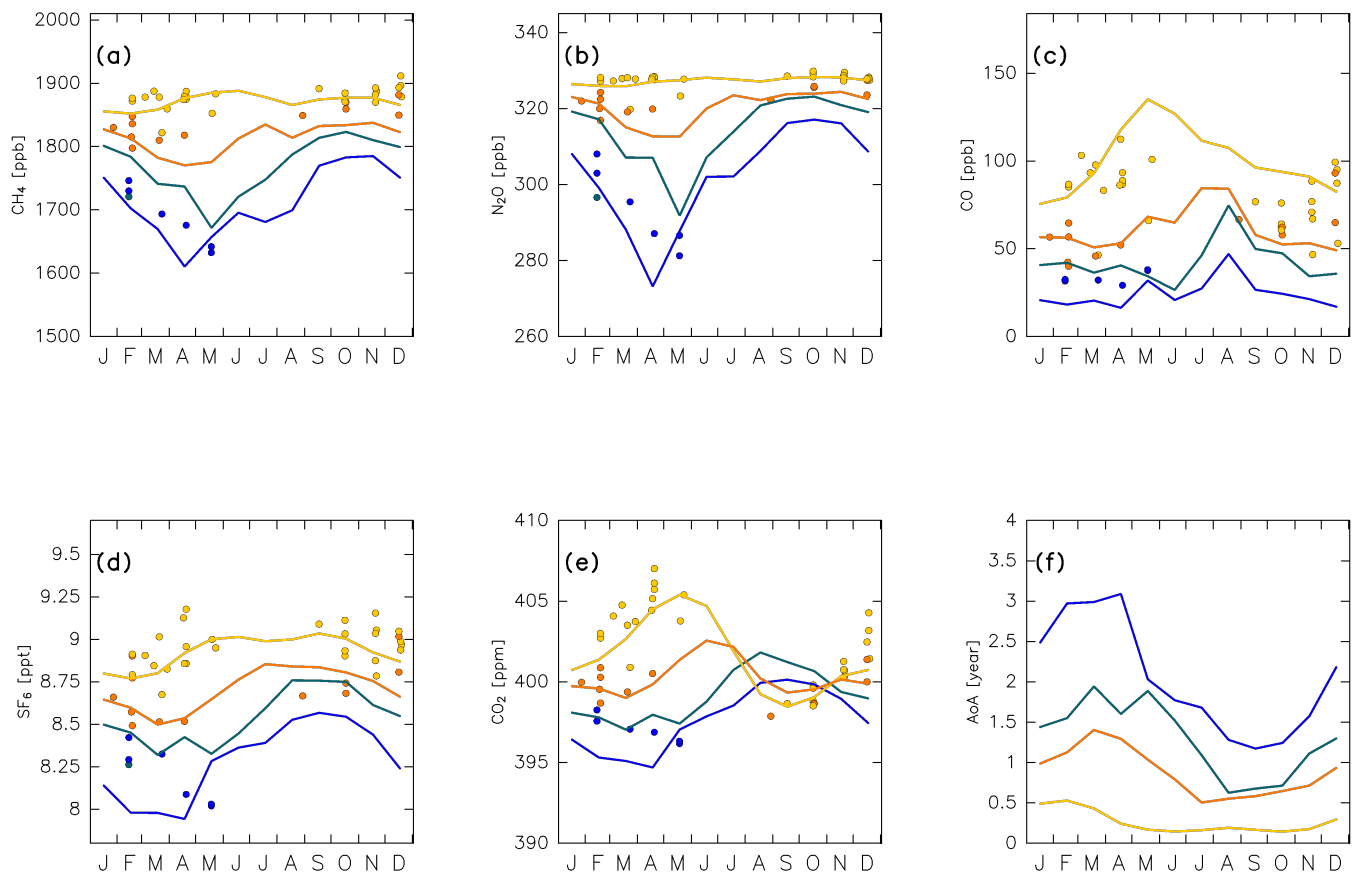
Figure 20: Seasonal variations in (a) CH₄, (b) N₂O, (c) CO, (d) SF₆, and (e) CO₂ mixing ratios estimated for the (green) mid-latitude upper ($\emptyset_{eq}$ = 45°N; θ = 370 K), (blue) high-latitude upper ($\emptyset_{eq}$ = 75°N; θ = 370 K), (yellow) mid-latitude lower ($\emptyset_{eq}$ = 45°N; θ = 320 K), and (orange) high-latitude lower ($\emptyset_{eq}$ = 75°N; θ = 320 K) ExUTLS superimposed on detrended CONTRAIL measurements, which are colour-coded according to measurements within ±5° in equivalent latitude and ±5 K in potential temperature of the reconstruction regions. Seasonal variations of the age of air (AoA) estimated for the same locations are shown in (f).
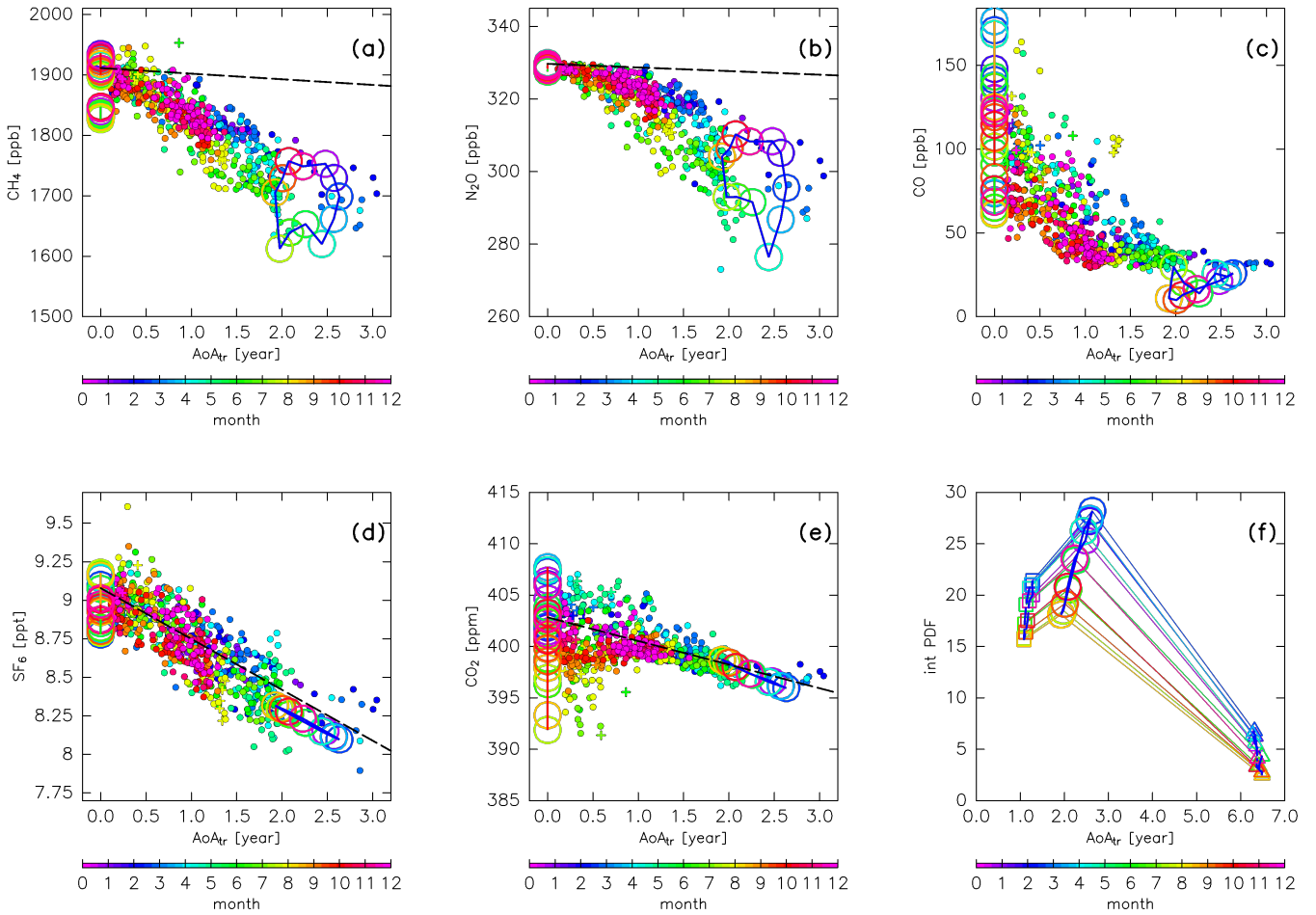
Figure 21: Scatter plots of the mean age of air (AoA) versus (a) CH₄, (b) N₂O, (c) CO, (d) SF₆, and (e) CO₂ mixing ratios measured by CONTRAIL (filled circles; colours indicate the month). Lines with open circles, coloured according to month, show the original compositions for (green) tropical tropospheric, (blue) stratospheric, (orange) mid-latitude LT, and (red) high-latitude LT air masses. Dashed lines in (a), (b), (d), and (e) show the sign-reversed trends of tropospheric CH₄ (−9.3 ppb/year), N₂O (−1.0 ppb/year), SF₆ (−0.33 ppt/year), and CO₂ (−2.3 ppm/year) with intercepts of the annual averaged mixing ratios at mid-latitudes for 2016 (1911 ppb, 330 ppb, 9.08 ppt, and 403 ppm), respectively. Mixing ratios estimated for stratospheric air masses in (a–e) are plotted after taking 3-month running averages to reduce fluctuations. Panel (f) shows the AoA estimated for air masses originating in the stratosphere (open circles), along with those estimated only for air masses passing through the deep (triangles) and shallow branches (squares) of the BDC. The ordinate is the integral of PDF of the "age spectrum" for each subset.
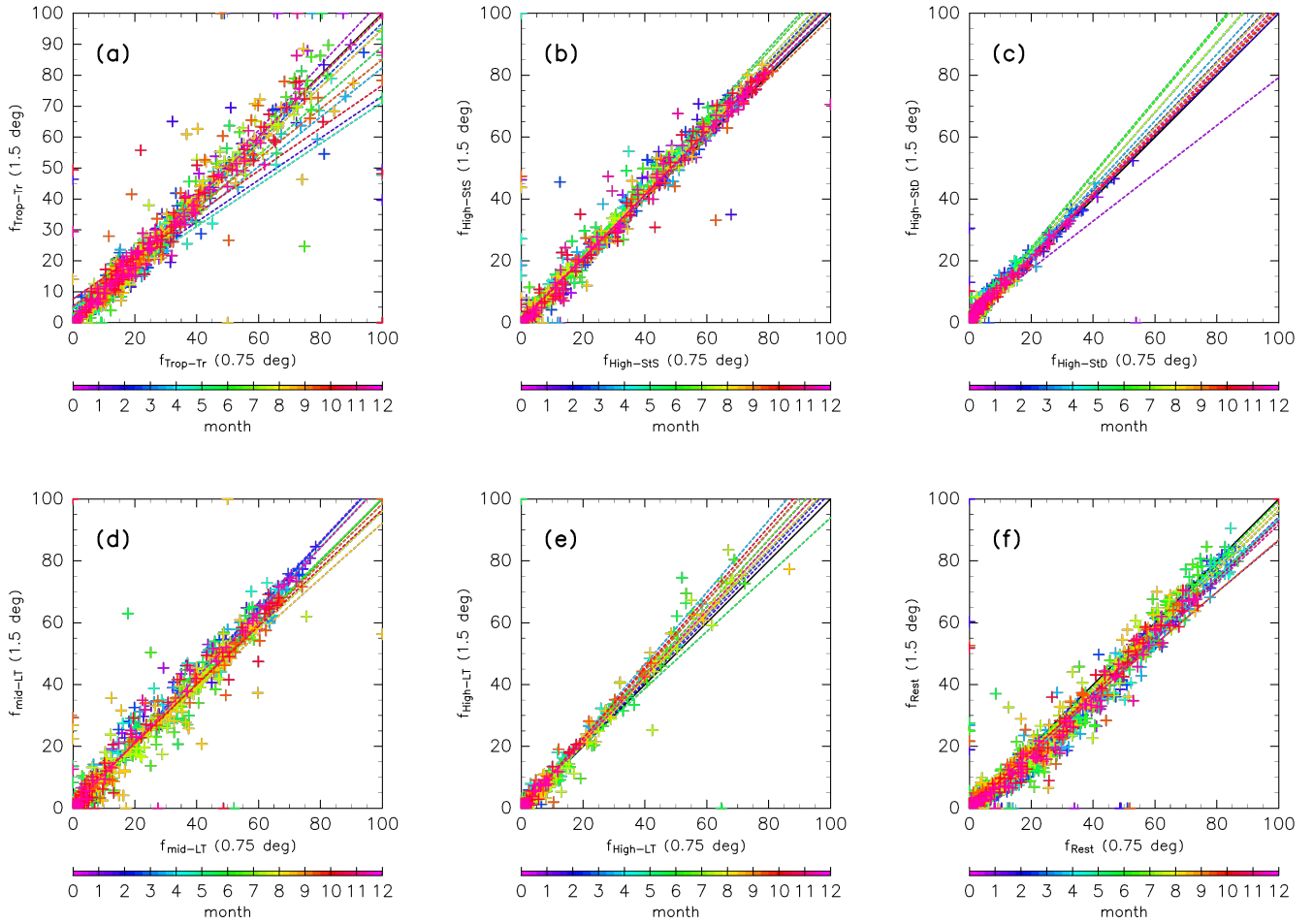
Figure A1: Scatter plots of origin fractions calculated using ERA-Interim data with a horizontal resolution of 0.75° and 60 model levels versus those with 1.5° horizontal resolution and 37 pressure levels. Both are estimated by 90-day trajectory calculations because of computing limitations. Crosses indicate mixing fractions evaluated for all bins in the $\emptyset_{eq}-\theta$ cross-sections shown in Figs 10–13 for (a) tropical tropospheric, (b) stratospheric (through the shallow branch of the BDC), (c) stratospheric (through the deep branch of the BDC), (d) mid-latitude LT, (e) high-latitude LT, and (f) unclassified air masses from 90-day trajectories. Colours indicate the month and dotted lines indicate the regression line for each month.
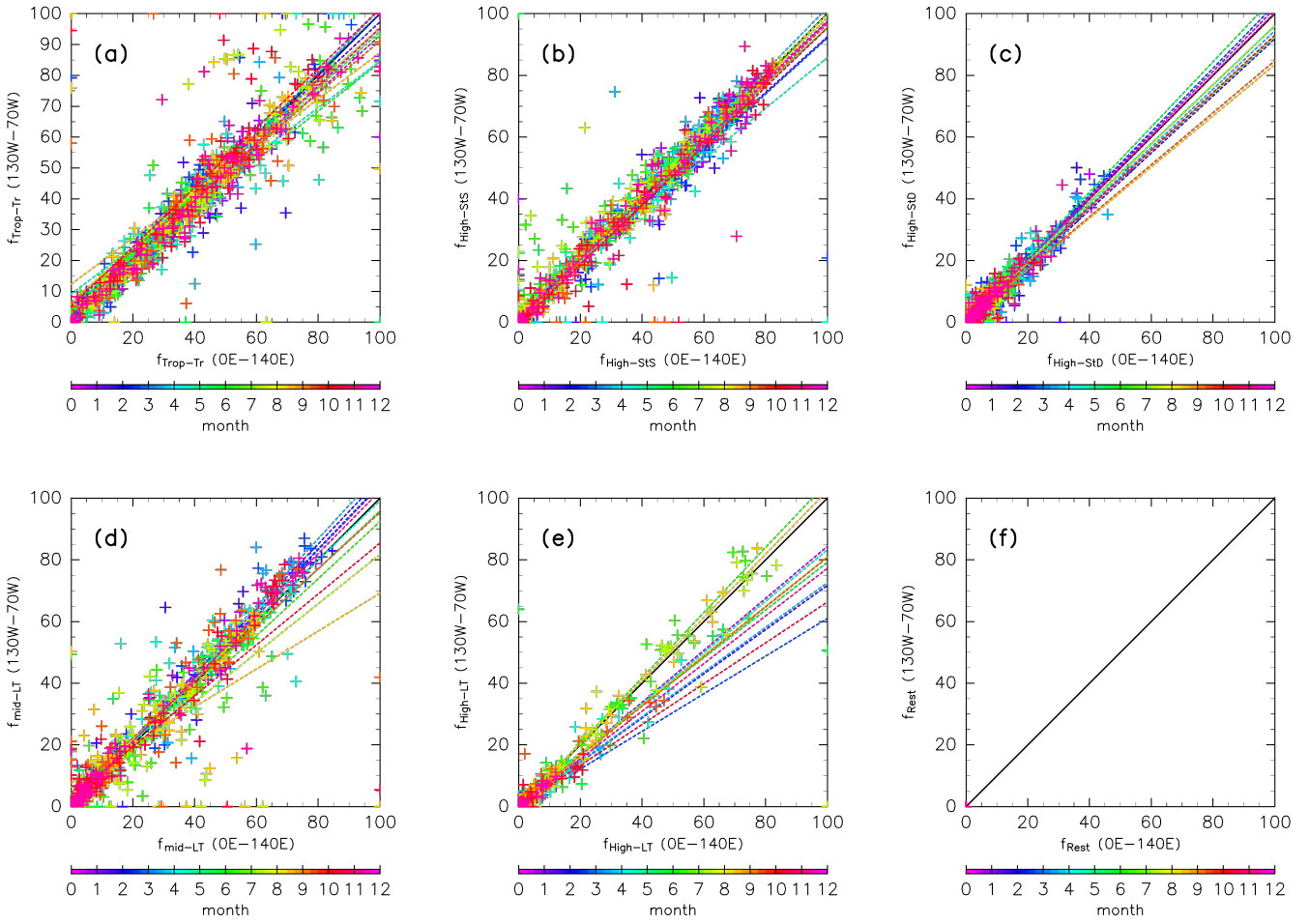
Figure A2: As in Fig. A1, but for origin fractions using 10-year trajectories calculated for the longitudinal region within 0° E–140° E (default) versus those for the region within 130° W–70° W.
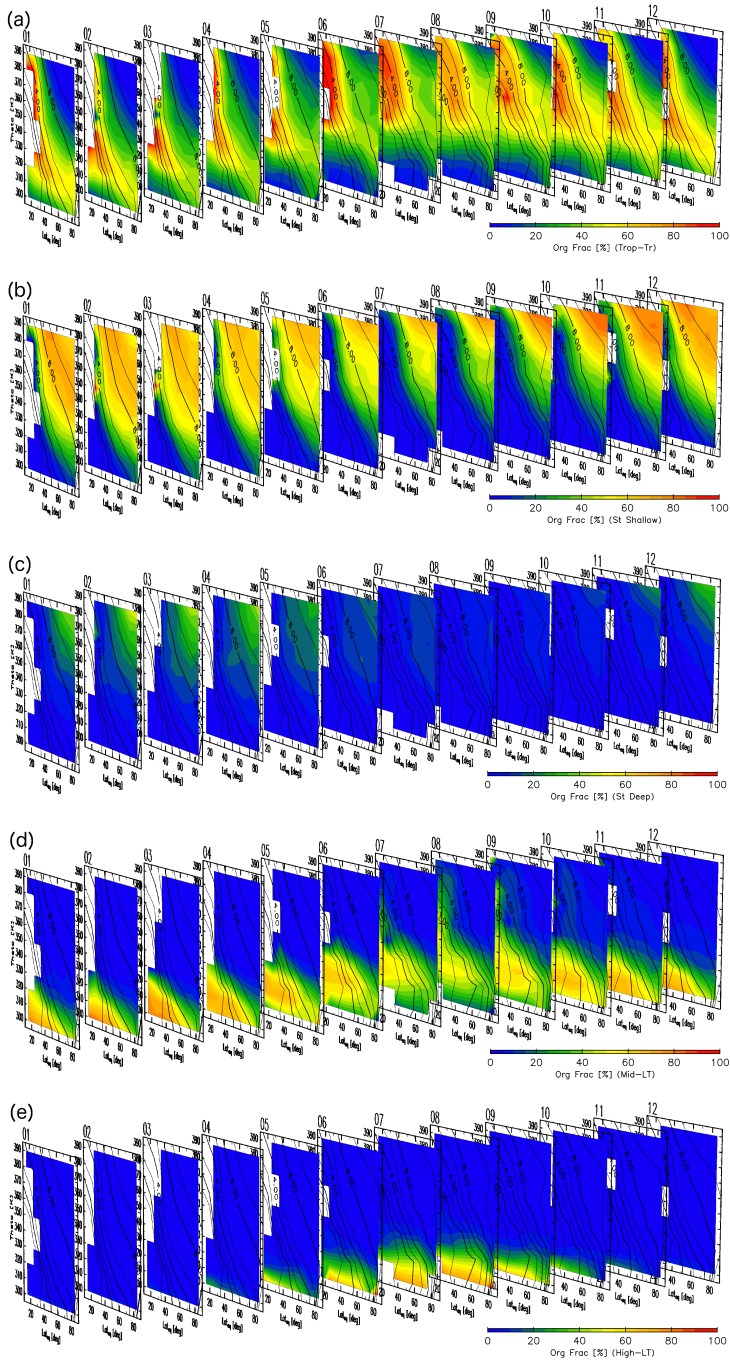
Figure B1: Origin fractions for (a) tropical tropospheric, (b) stratospheric (via the shallow branch of the BDC), (c) stratospheric (via the deep branch of the BDC), (d) mid-latitude LT, and (e) high-latitude LT air masses estimated for each month of the year with axes as in Figs 10–13. Black contours indicate monthly average potential vorticity during the period 2012–2016.
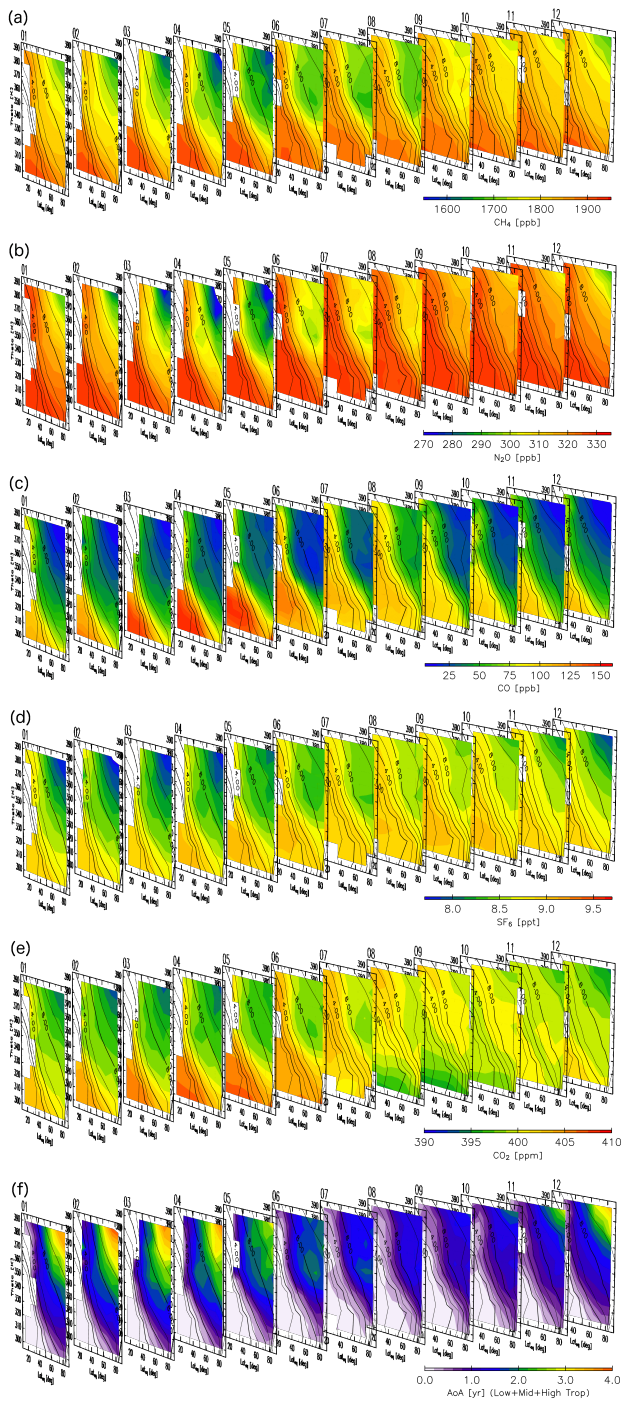
Figure B2: As in Fig. B1, but for reconstructions for (a) CH₄, (b) N₂O, (c) CO, (d) SF₆, and (e) CO₂, along with (f) the age of air (AoA) for each month.